

# **A study to halt the Crack Growth by combined action of Crack Stop Hole and Carbon Fibre Reinforced Polymer (CFRP) Laminates**

G Vinod Kumar

A Thesis Submitted to  
Indian Institute of Technology Hyderabad  
In Partial Fulfillment of the Requirements for  
The Degree of Master of Technology



भारतीय प्रौद्योगिकी संस्थान हैदराबाद  
Indian Institute of Technology Hyderabad

Department of Civil Engineering

July, 2016

## Declaration

I declare that this written submission represents my ideas in my own words, and where others' ideas or words have been included, I have adequately cited and referenced the original sources. I also declare that I have adhered to all principles of academic honesty and integrity and have not misrepresented or fabricated or falsified any idea/data/fact/source in my submission. I understand that any violation of the above will be a cause for disciplinary action by the Institute and can also evoke penal action from the sources that have thus not been properly cited, or from whom proper permission has not been taken when needed.



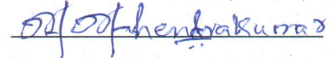
(Signature)

G Vinod Kumar

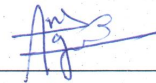
CE14MTECH11002

## Approval Sheet


This thesis entitled “**A study to halt the Crack Growth by combined action of Crack Stop Hole and Carbon Fibre Reinforced Polymer (CFRP) Laminates**” by G Vinod Kumar is approved for the degree of Master of Technology from IIT Hyderabad.



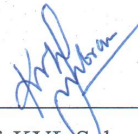
Dr Mahendra Kumar Madhavan  
Adviser



Dr Anil Agarwal  
Internal Examiner



Dr Saravanan B  
External Examiner



Prof. KVL Subramaniam  
Chairman

## **Acknowledgements**

I would like to thank Ministry of Human resources Development (MHRD), Government of India for providing financial support during my stay at IIT, Hyderabad. During last one year time, the guidance and assistance given by my thesis advisor Dr. Mahendrakumar Madhavan is highly acknowledged. I would like to thank Prof. K.V.L. Subramaniam, Dr. Anil Agarwal, Dr. Viswanath Chinthapenta and Dr Saravanan for reviewing the progress of my work. I am thankful for computational and experimental facilities provided by the department of civil engineering and Mechanical Engineering; IIT Hyderabad. I would like to thank my friends Mr Sashidhar Reddy, Mr Siva Ganesh and Mr Vijay Kumar for their time and valuable suggestions. I am thankful to my family, who helped me to pursue my Masters. I would like to thank all my friends for their support during my stay at IIT Hyderabad.

## **Abstract**

To arrest the crack propagation in structures subjected to fatigue load, drilling a hole ahead the crack tip is one of the most common repair technique. Due to site restrictions and geometrical constraints drilling an adequate size crack stop hole may not be possible. In such situations, to strengthen the undersized crack stop hole a carbon reinforced fiber polymer (CFRP) is attached to the structure. In the present study the effect of combined action of crack stop hole and CFRP laminates under static tensile loading is studied by using finite element analysis and validated by experimental studies. The finite element analysis is carried out in ANSYS 12.0 software and experimental studies are carried by universal testing machine (UTM) in Structural engineering laboratory, IIT Hyderabad.

Chapter 1 deals with the numerical study on the combined action of crack stop hole and symmetrically bonded CFRP patch in halting the crack propagation. A steel plate with an initial central crack and hole at crack tip is modelled, CFRP patches are attached on either sides of the cracked specimen. The numerical analysis is performed by using ANSYS 12.0 software. The areas of stressed regions after attaching different layers of CFRP are briefly explained for various crack inclinations subjected to four static tensile loads in the form of tables and figures.

Chapter 2 deals with the numerical study on the combined action of crack stop hole and asymmetrically bonded CFRP patch in halting the crack propagation. A steel plate with an initial central crack and hole at crack tip is modelled, CFRP patches are attached on one side of the cracked specimen. The numerical analysis is performed by using ANSYS 12.0 software. The areas of stressed regions after attaching different layers of CFRP are briefly explained for various crack inclinations subjected to four static tensile loads in the form of tables and figures.

Chapter 3 deals with the experimental study on the combined action of crack stop hole and asymmetrically bonded CFRP patch in halting the crack propagation. A total of 15 specimens are tested in which 5 are bare steel, 5 are asymmetrically

bonded and remaining five are symmetrically bonded specimens. The present study is carried out for 5 different crack stop hole radii and for 1 layer of CFRP. The results are again compared with the finite element analysis which shows the same behavior. The results are shown in the form of graphs and the efficiency of different repair techniques are compared.

## Nomenclature

|                       |   |
|-----------------------|---|
| CFRP                  | Carbon fibre reinforced polymer                           |
| CSIF                  | Crack stress intensity factor                             |
| ECFRP                 | Young's modulus of CFRP                                   |
| $E_{\text{steel}}$    | Young's modulus of steel                                  |
| $E_{\text{CFRP}}$     | Young's modulus of CFRP laminates                         |
| $K_I$                 | Stress intensity factor                                   |
| NSIF                  | Notch stress intensity factor                             |
| RF                    | Reduction factor  |
| $X_c$                 | Characteristic distance                                   |
| $\alpha$              | Gradient of stress distribution a head of crack stop hole |
| $\rho$                | Crack stop hole radii                                     |
| $\sigma_{\text{ys}}$  | Yield strength of steel                                   |
| $\sigma_{\text{app}}$ | Applied stress  |
| $\sigma_{\text{yy}}$  | Stress at characteristic distance                         |
| $2a$                  | Crack length  |

# Contents

|   |                                     |
|---|-------------------------------------|
| Declaration.....  | <b>Error! Bookmark not defined.</b> |
| Approval Sheet .....  | <b>Error! Bookmark not defined.</b> |
| Acknowledgements .....  | 1                                   |
| Abstract.....   | 2                                   |
| <b>Nomenclature .....</b>   | <b>4</b>                            |
| <b>1 Effect of crack stop hole and symmetrically bonded CFRP layers on yielded areas of steel plate .....</b>                     | <b>1</b>                            |
| 1.1 Introduction .....  | 1                                   |
| 1.1 Literature review.....  | 1                                   |
| 1.2.1 CFRP patches.....   | 1                                   |
| 1.2.2 Inclined cracks .....   | 3                                   |
| 1.3 Geometry and FE modelling.....  | 8                                   |
| 1.4 Results and discussion .....  | 9                                   |
| 1.4.1 25% Yield .....   | 10                                  |
| 1.4.2 50% Yield .....   | 10                                  |
| 1.1.5 75% Yiled .....   | 10                                  |
| 1.5 Example 1 .....   | 11                                  |
| 1.6 Refernces .....   | 14                                  |
| 1.7 Figures .....   | 14                                  |
| <b>2 Effect of crack stop hole and asymetrically bonded CFRP layers on yielded areas of steel plateCreating New Chapter .....</b> | <b>41</b>                           |
| 2.1 Introduction.....   | 41                                  |
| 2.2 Background.....   | 44                                  |
| 2.3 Geometry and FE modelling.....  | 49                                  |
| 2.4 Results and discussion .....  | 51                                  |
| 2.4.1 Effect of crack stop hole and CFRP layers .....   | 51                                  |
| 2.5 Calculation of crack stop hole radii .....  | 52                                  |
| 2.5.1 Example 1 .....   | 52                                  |
| 2.2.2 Example 2 .....   | 54                                  |



|          |  |           |
|----------|--|-----------|
| 2.6      | Refernces .....  | 57        |
| 2.7      | Figures .....  | 60        |
| <b>3</b> | <b>Experimental study to halt the crack propagation by combined action of crack stop hole and CFRP laminates .....</b> | <b>72</b> |
| 3.1      | Introduction .....   | 72        |
| 3.2      | Literature review.....   | 72        |
| 3.3      | Experimental Study .....   | 77        |
| 3.3.1    | Materials and specimen .....   | 77        |
| 3.3.2    | Material properties.....   | 77        |
| 3.3.3    | Coupon test .....  | 78        |
| 3.3.4    | Specimen preparation .....   | 78        |
| 3.3.5    | Static tensile testing .....   | 79        |
| 3.4      | Experimental results .....   | 79        |
| 3.4.1    | NSIF calculation .....   | 80        |
| 3.4.2    | $X_c$ calculation.....   | 81        |
| 3.4.3    | Stress gradient calcuation .....   | 81        |
| 3.4.4    | Optimum crack stop hole radii calculation.....   | 82        |
| 3.4.5    | Stress intensity factor vs crack stop hole radii.....  | 82        |
| 3.4.6    | Reduction factor.....  | 83        |
| 3.5      | verification of experimental results by using FEA .....  | 83        |
| 3.5.1    | Geometry and finite element modelling .....  | 83        |
| 3.6      | Results and discussion .....   | 84        |
| 3.7      | Conclusion .....   | 85        |
| 3.8      | Refernces .....  | 87        |
| 3.9      | Figures .....  | 89        |

# Chapter 1

## **Effect of crack stop hole and symmetrically bonded CFRP layers on yielded areas of steel plate**

### **1.1 Introduction**

Due to fatigue load, cracks originate in structural members leading to a rise in stress close to the crack tip. If the cracked specimen is left unrepaired for a long time it leads to sudden failure. To prevent such occurrence, various retrofitting techniques are employed which can be broadly classified into two groups (Shield et al, 2004): (a) Local retrofitting techniques which include crack stop holes, peening, Gas Tungsten Arc (GTA) welding that modify the local stress state and (b) Global retrofitting techniques that include strengthening with steel plate or composite laminates. In the present approach, a combination of crack stop hole and CFRP is used to arrest crack propagation in structures where the direction of crack is inclined with respect to the direction of load.

### **1.2 Literature Review**

#### **1.2.1 CFRP Patches**

Several researchers have studied the effectiveness of composites as a repair technique to prevent crack propagation in structures subjected to fatigue loading by focusing on reducing the stress intensity factor. The results from Chandra et al (1985) indicate that the application of patch results in substantial reduction in SIF and are more effective when the patch is placed at a little distance inwards of the crack tip, not the crack tip itself or ahead of the crack. Heller et al (1989) carried out

experimental studies on the use of a bonded sleeve insert and/or a bonded composite patch to reduce the rate of fatigue crack propagation. The results indicate that significant increases in fatigue life can be achieved using a bonded sleeve alone. However, the additional use of an externally bonded patch produces an increase in the fatigue life of the specimens of between 1 to 2 orders of magnitude. Achour et al. (2003) performed finite element analysis to understand the effect of composite patches in retarding the crack from semi-circular notches. The stress concentration factor was decreased by 30% due to the patch. The studies also indicate that the properties of patch system such as patch thickness and adhesive properties need to be optimized for the effectiveness of the repair.

Chung and Wang (2003a) carried out experimental investigations on the effect of single sided composite material patch repair to characterize the fatigue crack growth behavior in thick aluminium panels. The results indicate that the fatigue life of patched plate increases about 4-6 times compared to the un-patched plate. In addition, when the patch length is 1.5 times longer than the crack length, the longest fatigue life can be obtained. Okafor et al (2005) studied the single sided composite patch repair of a cracked aluminium panel using boron/epoxy patch for two different ply configurations (5 ply and 6 ply). Uniaxial tensile testing was carried out to validate the analytical results. The experimental results indicate that the maximum skin stress decreases significantly after the application of the patch and the region of maximum skin stress shifts from the crack front for an unpatched panel to the patch edges for a patched one.

Ramji and Srilakshmi (2012) studied numerically the performance of single- and double-sided patch on center-cracked aluminium panel for various parameters such as patch layup, patch thickness and patch material. The results indicate the double sided repair is more effective than a single sided repair. Similar studies on the comparison between single and double sided patch were carried out by Albedah et al. (2003) and Belhouari et al. (2004). The results show that the single sided repair is effective only when crack length is less and the difference between double sided repair and single sided repair becomes constant as the patch thickness is increased. The results hold only if bending of plate is not considered due to asymmetric difference in stiffness in case of single sided repair.

### **1.2.2 Inclined Cracks**

The present study is focused on centreline inclined crack of varying degrees with various crack stop hole radii at crack ends with a double sided CFRP patch subjected to four different tensile loads. When the crack is inclined with loading direction, it undergoes a mixed mode of cracking involving mode I and mode II (Anderson, 2005). The stress intensity factor corresponding to mode I is significantly reduced due to the presence of the patch. The effectiveness of the patch can be further increased by increasing the patch thickness. The following literature focuses on the research work carried on crack propagation due to mixed mode conditions.

Erdogan and Sih (1962) examined theoretically and experimentally the behavior of crack extension in a large plate subjected to general plane loading. The results

indicate that under skew-symmetric plane loading of brittle materials the “sliding” or the crack extension in its own plane does not take place; instead crack grows in the direction approximately 70 degree from the plane of the crack. Tanaka (1973) studied the effect of initial crack inclination ( $30^\circ$ ,  $45^\circ$ ,  $72^\circ$  and  $90^\circ$ ) on aluminium sheets when subjected to cyclic stress with a stress ratio  $R = 0.65$ . The results indicate that the threshold condition for the non-propagation of the initial crack was given by a quadratic form in terms of stress intensity factors for mode I and mode II. In addition, the direction of fatigue crack extension from the inclined crack was roughly perpendicular to the tensile axis at stress ranges just above the threshold value for non-propagation. On the other hand, at stress ranges 1.6 times higher than the threshold values, the crack grew in the direction of initial crack.

Jones and Callinan (1981) carried out numerical investigation into the behavior of cracked sheets which are patched with an overlay of composite material. The study results in the development of guidelines with regard to optimum location, size and shape of patches based on 3 main considerations such as reduction in SIF at crack tip, maximum fiber stress in the patch and the maximum shear stress in the adhesive bond between patch and sheet.

Rose (1982) studied the behavior of a crack with reinforcing sheets bonded to its face and subjected to a uniformly distributed tensile load at right-angles to the crack. The results indicate that the crack extension force has a finite value, provided that the reinforced structure can still carry the load if the crack runs across the whole plate, cutting it in half.

Sethuraman and Maiti (1989) developed a method to determine the stress intensity factors under mixed mode loading of a crack-stiffened panel. The parametric studies carried out by the authors indicate that the SIF depends on patch location, patch length, shear modulus of the stiffener and adhesive and thickness of adhesive.

Domazet (1996) examined the efficiency of several crack retarding methods and concluded that crack stop hole in combination with CFRP patches applied to both sides, are the best fatigue crack retardation methods for all loading conditions.

Kumar and Hakeem (2000) carried out a shape optimization study of symmetric (balanced) composite patch to a centre cracked metallic sheet using crack tip stress intensity factor (SIF) as a parameter. The results indicate that a skewed patch is the most optimum patch design followed by a rectangular patch and that increasing the patch thickness has a greater effect than the patch area. Khan and Khraisheh (2000) carried out a detailed analysis of mixed mode I-II crack initiation angles under different loading conditions. The experimental results from uniaxial tension test indicate that the results are in somewhat good agreement with most criteria for higher crack inclination angles whereas for low inclination angles, no particular criterion is favoured. The scatter in the results indicates the need for a detailed experimental investigation to identify variables that have a strong influence on crack initiation angles. Bouiadjra and Serier (2002) studied numerically the behavior of repaired cracks with bonded composite patches in mode I and mixed mode by computing the SIF's at the crack tip. The results indicate that the SIF exhibits an asymptotic behavior as the crack length increases. Further, in mixed mode, the obtained results show that the mode I SIF is more affected by the presence of patch than that of mode II.

Chung and Wang (2002) analysed the stress intensity factor at a skin/stiffener structure with an inclined central crack repaired by composites. The investigation characterized numerically the fracture behavior and crack growth behavior at an inclined crack using maximum tangential stress criterion. The results indicate that the mode I SIF's are rapidly decreased as the angle between the loading direction and inclined crack was decreased.

Chung and Wang (2003b) studied experimentally the fatigue crack growth behavior of aluminium plates reinforced with composite material patch with five ( $0^\circ$ ,  $15^\circ$ ,  $30^\circ$ ,  $45^\circ$  and  $60^\circ$ ) different crack inclinations. The results indicate that the fatigue life of patched plate with inclined crack increased approximately 2.4-5.0 times compared to no-patched plate. In addition, the maximum effect of patch was obtained from the plate with  $0^\circ$  inclined crack and the effect was relatively small in  $30^\circ$  and  $45^\circ$  inclined crack. The results also indicate that the fatigue life of the inclined crack decreased as the inclined angle increased from  $0^\circ$ - $30^\circ$ . This is due to the fact that, in the inclined angle range, mode I load dominated the crack propagation and also as the inclined angle increased the crack reached the patch boundary faster, the fatigue was decreased. On the other hand, as the incline angle increased further from  $30^\circ$ - $60^\circ$ , the fatigue life increased. This is due to the fact that the mode II was increased while the mode I load, which is the main cause of crack propagation, was decreased.

Song and Shieh (2004) investigated the improvement in crack initiation life and the total fatigue life in aluminium alloy and stainless steel due to stop drilling procedure. The results indicate that larger the stop-hole diameter, the larger the crack initiation lives due to lower stress gradients and stress concentrations. The results show that

by drilling a hole of size 3mm the fatigue life has been increased to 443% and 174% in case of aluminium alloy and stainless steel respectively. Hossein et al. (2006) developed a procedure to obtain the crack trajectories using dynamic mesh generation for repaired panels in both mode I and mixed mode conditions. The results indicate that the fatigue crack growth life obtained from the developed procedure is compatible with the experimental results for mode I conditions and non-conservative in some cases. The results also indicate that while the J-integral values at the mid-plane of the cracked plates reduce with increasing patch thickness for both mode-I and mixed-mode crack loading conditions, it does not have considerable effect on the crack propagation path.

Ramji et al (2013) carried out finite element analysis to understand the patch shape on inclined center crack having a crack inclination of  $45^\circ$ . The results indicate a drastic reduction in mode I and mode II SIF value irrespective of patch shape for a double sided patch. The results also indicate that an extended octagonal CFRP patch is most effective for repairing inclined cracked panel. Alemdar et al. (2013) carried out experiments on 15 steel plates to investigate the effectiveness of CFRP in repairing pre-existing fatigue cracks with varying thickness of overlays. The results indicate that an increase in axial stiffness ratio from 0 to 0.4 could increase the fatigue life by a factor of 10 for the most extreme conditions, and with an optimal axial stiffness ratio infinite fatigue life may be reached. The results also indicate that the fatigue life of steel specimens studied were dependent on both axial stiffness and applied stress range.



The above literature indicate the research work carried out in the area of inclined crack for both patched and unpatched plates but to the authors knowledge literatures corresponding to inclined cracks with crack stop holes with CFRP patches are none. This indicates that there is a need to study the combined action of crack stop hole and CFRP application as a repair technique on inclined crack.

### **1.3 Geometry and FE modelling**

The specimen geometry is taken from the experimental work of Barsom and Nicol (1974) and modified from double edge notch specimen to central crack specimen to model the effect of crack stop hole. The magnitudes of loads applied are 41.2 MPa (6 ksi), 62 MPa (9 ksi), 82.7 MPa (12 ksi), 103.4 MPa (15 ksi) which were reported as loads that the bridge girders are generally subjected to (Fisher, 1980). The connection between CFRP, steel plate and CFRP, adhesive are modeled using bonded contact. In bonded contact, contacting surfaces are assumed to be glued together throughout the analysis. To create bonded contact, contact and target elements needs to be defined on the faces of elements, where they come into contact. In this study, multipoint constraint (MPC) algorithm is used for bonded contact. CFRP laminate is modeled as an orthotropic material. The CFRP material properties are taken from Ramji et al (2013) and in the present study, the number of CFRP layers varied are 10 which range from 0 to 10 numbers. The thickness of the lamina reported in the reference is 0.375mm and CFRP patch length (l) is taken as 127 mm based on the numerical study by Zhao and Zhang (2007).

Incremental meshing as given by Nakmura and Parks (1989) is employed around the hole to capture the sharp stress gradient because the value of stress at the edge of the hole is sensitive to element size. The number of elements used around the hole is 6 elements in thickness direction shown in Fig. 1 and 20 elements in radial direction and 48 elements in angular direction as shown in Fig. 1. Although the applied loads are less than the yield stress of steel, localized yielding occurs at crack tip. Therefore, to take into account the local yielding behavior, a nonlinear Finite Element Analysis (FEA) is carried out in this research work using ANSYS 12.0 software. The material model used for Steel is Multi Linear Isotropic hardening. For modeling all components (i.e. steel plate, adhesive, and CFRP plate) Solid 186 element is used. Solid 186 element has mid side nodes and it performs better in stress singularity regions and for nonlinear analysis.

#### **1.4 Results and discussion**

This numerical study is aimed at studying the combined action of crack stop hole and the CFRP patch in arriving at the appropriate crack stop hole radius, number of CFRP layers when subjected to static tensile load.

After running analysis, the position of nodes are collected according to the stress boundaries. The nodes are plotted in the AUTOCAD 2012 software and areas of the regions are calculated by joining the nodes.

Calculated the area which is greater than the 25% yield, 50% yield and 75% yield when plate is subjected to four different loads 41.2MPa, 62MPa, 82.7MPa and 103.4MPa. For various crack inclinations (0, 15, 30, 45, 60).

#### **1.4.1 25% yield (>75MPa)**

Yield strength of the plate is 303MPa. In this 25% is approximately 75MPa. Calculated the area of stress region of plate which is greater than 75MPa when subjected to four different loads. After go on attaching the CFRP sheets to the plate, 1 layer of CFRP cannot make a big difference from bare steel specimen. The area will be reducing gradually after attaching the CFRP layers. After attaching 10 layers of CFRP the stress region became negligible which is shown in Fig. 2 and Fig. 3.

#### **1.4.2 50% yield (>150MPa)**

Yield strength of the plate is 303MPa. In this 50% is approximately 150MPa. Calculated the area of stress region of plate which is greater than 150MPa when subjected to four different loads. After go on attaching the CFRP sheets to the plate, the area will be reducing gradually. After attaching 3 layers of CFRP the stress region became negligible which is shown in Fig. 4 and Fig. 5.

#### **1.4.3 75% yield (225MPa)**

Yield strength of the plate is 303MPa. In this 75% is approximately 225MPa. Calculated the area of stress region of plate which is greater than 225MPa when subjected to four different loads. After attaching a CFRP sheet to the plate, the stress region became negligible which is shown in Fig 6 and Fig 7.

For any inclination of cracks the area of stressed regions were decreasing after attaching the CFRP patches.

Layer wise areas are shown as tabular columns in Fig. 8 to Fig. 17

### 1.5 Example

Consider a load of 75 MPa acting on a specimen with center crack of length (2a) 63.5 mm. The steel and CFRP properties and dimensions are the same as considered in this paper. The site conditions are such that the maximum radius of hole that can be drilled is 10mm. Determine the number of CFRP layers required to arrest the crack.

*Solution:* The solution to the problem is carried out in a step by step format as shown below:

1. Calculate  $K_I/\rho^\alpha$  from given equation below of a bare steel specimen and plot the variation of the same with respect to various crack stop hole radii (0.375 inch to 1/32 inch) as shown in Fig. 19.

$$K_\rho = \sigma_{yy}(X_c) * \sqrt{2\pi} \left( X_c + \frac{\rho}{2} \right)^\alpha$$

2. Plot the threshold line as per equation shown below which is given by Barsom (1974), in the same plot of  $K_I/\rho^\alpha$  versus crack stop hole radii to determine the threshold radius. As there is no intersection between the threshold line and the bare steel specimen curve obtained from FEA indicating that a CFRP patch is mandatory (crack stop hole alone is not enough) to reduce the SIF.

$$\frac{K_I}{\sqrt{\rho}} = 10\sqrt{\sigma_{ys}}$$

3. From the given conditions, as a start it is assumed that 1 layer of the CFRP patch with a crack stop hole radii of 9.525 mm is required to arrest a crack.

4. Input the parameters 2a (63.5 mm),  $\rho$  (9.525 mm) and  $\sigma_{applied}$  (75 MPa) in equation shown below and determine coefficients  $a$  through  $e$  by using

corresponding  $p_0$  through  $p_{16}$  for each coefficient using table (showing variation of  $p_0$  to  $p_8$  with coefficients  $a, b, c, d$  and  $e$ ) which is shown below

$$p_0 + p_1 * x + p_2 * y + p_3 * x^2 + p_4 * y^2 + p_5 * x * y + p_6 * x^2 * y + p_7 * x * y^2 + p_8 * y^3$$

5. Using the coefficients  $a$  through  $e$  obtained from Step 4 and Stress Ratio from ratio shown in Fig. 18, calculate  $RF$  using equation shown below. The  $RF$  value comes to around 0.74.

$$\text{Reduction factor} = \frac{(K_I / \rho^\alpha) \text{with CFRP}}{(K_I / \rho^\alpha) \text{w/o CFRP}}$$

$$RF = a (SR^5) + b (SR^4) + c (SR^3) + d (SR^2) + e (SR) + 1$$

6. From figure below, the value of  $K_I / \rho^\alpha$  of a bare steel specimen with crack stop hole radius of 9.525 mm is approximately 572.36 MPa. The corresponding value of specimen reinforced with 1 CFRP layer will be 423.54 MPa ( $0.74 \times 572.36$ ).

7. The reduced  $K_I / \rho^\alpha$  value (423.54 MPa) is now compared with  $10 \sqrt{\sigma_{ys}}$  (477 MPa). This value (477 MPa) is greater than reduced  $K_I / \rho^\alpha$  value (423.54 MPa) which indicates that 1 layer of CFRP with 9.525 mm radius may or may not result in crack re-initiation because 423.54 is very near to the yield strength

8. Since 423.54 is very near to the yield strength, consider two layers of CFRP. On repeating the same procedure shown above the  $RF$  value comes around 0.5779.

9. The value of  $K_I / \rho^\alpha$  of a bare steel specimen with crack stop hole radius of 9.525 mm is approximately 572.36 MPa. The corresponding value of specimen reinforced with 2 CFRP layers will be 330.76 MPa ( $0.5779 \times 572.36$ ).

10. The reduced  $K_I / \rho^a$  value (330.76 MPa) is now compared with  $10\sqrt{\sigma_{ys}}$  (477 MPa). This value (477 MPa) is greater than reduced  $K_I / \rho^a$  value (330.76 MPa) which indicates that 2 layers of CFRP with 9.525 mm radius will not result in crack re-initiation. Since the site conditions in the problem permit up to 10 mm crack stop hole radius, the assumed 2 layers of CFRP reinforcement with 9.525 mm crack stop hole radius is valid.

A nonlinear FEA carried out for the above conditions ( $2a = 63.5$  mm,  $\rho = 9.525$  mm,  $SR = 0, 0.08, 0.16$ , and load = 75 MPa). The values calculated for  $K_I / \rho^a$  of the bare steel specimen and patched specimen with 1, 2, layers are 569.09 MPa, 435.31 MPa and 338.01 MPa, respectively. The corresponding RF values are 1, 0.76 and 0.59 respectively. It can be observed that the difference is 2.63% and 1.21% between proposed equation and FEA for a SR of 0.08 and 0.16 respectively, indicating the accuracy of the proposed equation.

## 1.6 References

Achour T, Bachir BB, Series B (2003), “Numerical analysis of the performance of the bonded composite patch in reducing stress concentration and repairing crack at notch”, *Computational Computational Material Science*, 28 (1): 41–48.

Albedah A, Bachir BB, Mhamdia R, Benyahia F, Es-Saheb Es M (2011), “Comparison between double and single sided bonded composite repair with circular shape”, *Materials and Design*, 32: 996–1000.

Alemdar F, Gangel R, Matamoros A, Bennett C, Barrett-Gonzalez R, Rolfe ST, Liu H (2013), “Use of CFRP overlays to repair fatigue damage in steel plates under tension loading”, *J. compos. constr.*, 18 (4): 04013052.

Anderson TL (2005), “Fracture Mechanics Fundamentals and Application”, Third edition, Taylor and Francis group, LLC.

Bachir Bouiadjra B, Belhouari M, Series B, (2002), “Computation of the stress intensity factors for repaired cracks with bonded composite patch in mode I and mixed mode”, *Compos. Struct.*, 10.1016/S0263-8223(02)00023-5.

Barsom JM (1985), “Fracture Mechanics –Fatigue and fracture”, *Metals Handbook – Desk 398 Edition*, American Society for Metals, Metals Park, Ohio.

Barsom JM, McNicol RC (1974), “Effect of stress concentration on fatigue –cracks initiation in HY-130 steel”, *Fracture Toughness and Slow-Stable Cracking*, 4STM STP 559, 402 American Society for Testing and Materials, 183-204.

Belhouari M, Bachir BB, Megueni M, Kaddouari K (2004), “Comparison of double and single bonded repairs to symmetric composite structures”, *Compos. Struct.*, 65: 47–53.

Boukharouba T, Tamine T, Niu L, Chehimi C, Pluvinage G (1995), “The use of notch stress intensity factor as a fatigue crack initiation parameter”, *Eng. Fract. Mech.*, 52(3): 503-512.

Chung and Yang. (2002), “Fracture mechanics analysis on the bonded repair of a skin/stiffener with an inclined central crack” *Compos. Struct.*, 10.1016/S0263-8223(01)00163-5.

Chung and Yang (2003), “.A study on the fatigue crack growth behavior of thick aluminum panels repaired with a composite patch”, *Compos. Struct.*, 10.1016/S0263-8223(02)00338-0.

Chung and Yang (2003), “Mixed mode fatigue crack growth in aluminum plates with composite patches”, *International J. Fatigue*, 25 (2003) 325–333.

Creager M, and Paris PC (1967) , “Elastic field equations for blunt cracks with reference to stress corrosion cracking”, *International J. Fract. Mech.*, 3(4): 247-252.

Domazet Z (1996), “Comparison of fatigue crack retardation methods”, *Eng. Failure Analysis*, 3 (2): 137–147.

Erdogan F and Sih GC, (1962), “On the Crack Extension in Plates under Plane Loading and Transverse Shear”, *J. Basic Eng.*, 10.1115/1.3656897



Fisher JW, Barthelemy BM, Mertz DR, Edinger JA (1980), "Fatigue behaviour of full scale welded bridge attachments", Fritz Laboratory Reports, 1980 NCHR 12-15(3), (80-29).

Heller M, Hill TG, Williams JF, Jones R (2003), "Increasing the fatigue life of cracked fastener holes using bonded repairs", Theoretical and Applied Fracture Mechanics, 10.1016/0167-8442(89)90020-7.

Hosseini HT, Bijan Mohammadi, Hamid Reza Daghyani, (2006), "Mixed-mode fracture analysis of aluminium repaired panels using composite patches" Compos. Science and Technology, 10.1016/j.compscitech.2005.04.028.

Irwin GR (1957), "Analysis of stresses and strains near the end of a crack transversing a plate". Transactions, ASME, J. Applied Mechanics, 25: 361-364.

Jones R, Callinan RJ, (1981), "A design study in crack patching" Fibre Science and Technology 10.1016/0015-0568(81)90035-X.

Khan SMA, Khraisheh MK, (2000), "Analysis of mixed mode crack initiation angles under various loading conditions", Eng. Fract. Mech., 67 (2000) 397 – 419.

Kumar AM, Hakeem SA (2000), "Optimum design of symmetric composite patch repair to center cracked metallic sheet", Compos Struct., 10.1016/S0263-8223(00)00005-2.

Nakamura T, Parks DM (1989), "Antisymmetrical 3D stress field near the crack front of a thin elastic plate", International J. Solids and Structures 25 (12): 1411-1426.

Okafor C, Navdeep Singh, Enemuoh UE, Rao SV (2005), "Design, analysis and performance of adhesively bonded composite patch repair of cracked aluminum aircraft panels" *Compos. Struct.*, 10.1016/j.compstruct.2005.02.023.

Paris CP and Sih GC (1965), "Stress analysis of cracks. Fracture Toughness Testing and its Applications", ASTM STP 381, American Society for Testing and Materials, Philadelphia.

Ramesh C, Murthy MVV, Ramamurthy TS, Rao AK, (1985), "Analytical estimation of stress intensity factors in patched cracked plates", *Eng. Fract. Mech.*, 10.1016/S0013-7944(85)80041-2.

Ramji M, Srilakshmi R, Bhanu Prakash M (2013), "Towards optimization of patch shape on the performance of bonded composite repair using FEM", *Compos.: Part B* 45 (2013) 710–720.

Ramji M, Srilakshmi R (2012), "Design of composite patch reinforcement applied to mixed mode cracked panel using FEA" *J. of Reinforced Plastics and Compos.*

Rose LRF, (1982), "A cracked plate repaired by bonded reinforcements" *International J. of fract.*, 18 (1982) 135-144.

Sethuraman R, Maiti SK. (2003), "Determination of Mixed Mode Stress Intensity Factors for a Crack-stiffened Panel", *Eng. Fract. Mech.*, 10.1016/0013-7944(89)90086-6.

Shield C, Hajjar J, Nozaka K (2004), “Repair of fatigued steel bridge girders with carbon fiber strips”. Report no-MN/RC–2002-04, Minnesota Department of Transportation.

Song PS, Shieh YL (2004), “Stop drilling procedure for fatigue life improvement”, *International J. Fatigue*, 26(12): 1333–1339.

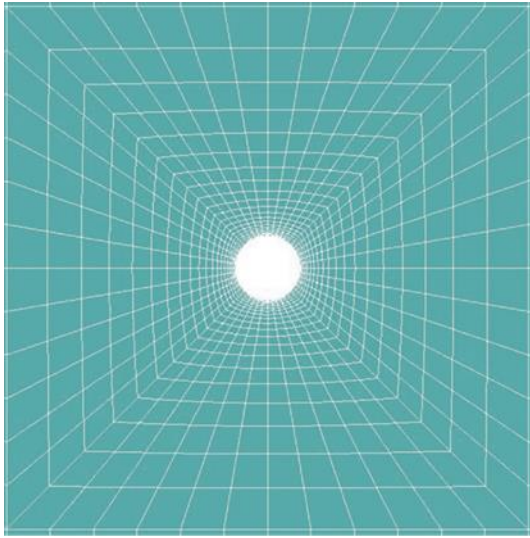
Tanaka K, (1973), “Fatigue crack propagation from a crack inclined to the cyclic tensile axis” *Eng. Fract. Mech.*, 10.1016/0013-7944(74)90007-1.

Zhao XL, Zhang L. (2007), “State-of-the-art review on FRP strengthened steel structures”, *Eng. Struct.*, 29 (8): 1808–1823.

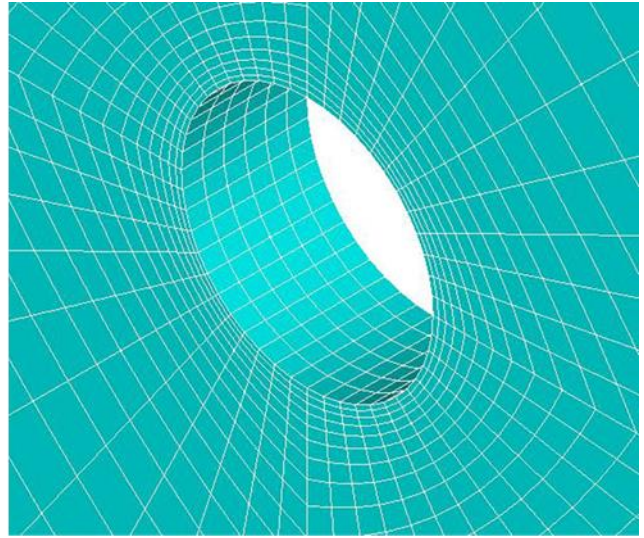
## 1.7 Figure captions

Figure 1(a) and (b): Meshing around the crack stop hole

- Figure 2: 25% Yield areas subjected to 41.2 MPa for various inclinations
- Figure 3: 25% Yield areas subjected to 103.4 MPa for various inclinations
- Figure 4: 50% Yield areas subjected to 41.2 MPa for various inclinations
- Figure 5: 50% Yield areas subjected to 103.4 MPa for various inclinations
- Figure 6: 75% Yield areas subjected to 41.2 MPa for various inclinations
- Figure 7: 75% Yield areas subjected to 103.4 MPa for various inclinations
- Figure 8: Areas of 0 degree crack subjected to 62MPa load
- Figure 9: Areas of 15 degree crack subjected to 62MPa load
- Figure 10: Areas of 30 degree crack subjected to 62MPa load
- Figure 11: Areas of 45 degree crack subjected to 62MPa load
- Figure 12: Areas of 60 degree crack subjected to 62MPa load
- Figure 13: Areas of 0 degree crack subjected to 82.7MPa load
- Figure 14: Areas of 15 degree crack subjected to 82.7MPa load
- Figure 15: Areas of 30 degree crack subjected to 82.7MPa load
- Figure 16: Areas of 45 degree crack subjected to 82.7MPa load
- Figure 17: Areas of 60 degree crack subjected to 82.7MPa load
- Figure 18: Variation of  $p_0$  to  $p_8$  with coefficients a, b, c, d and e
- Figure 19: Calculation of optimum crack stop hole radius

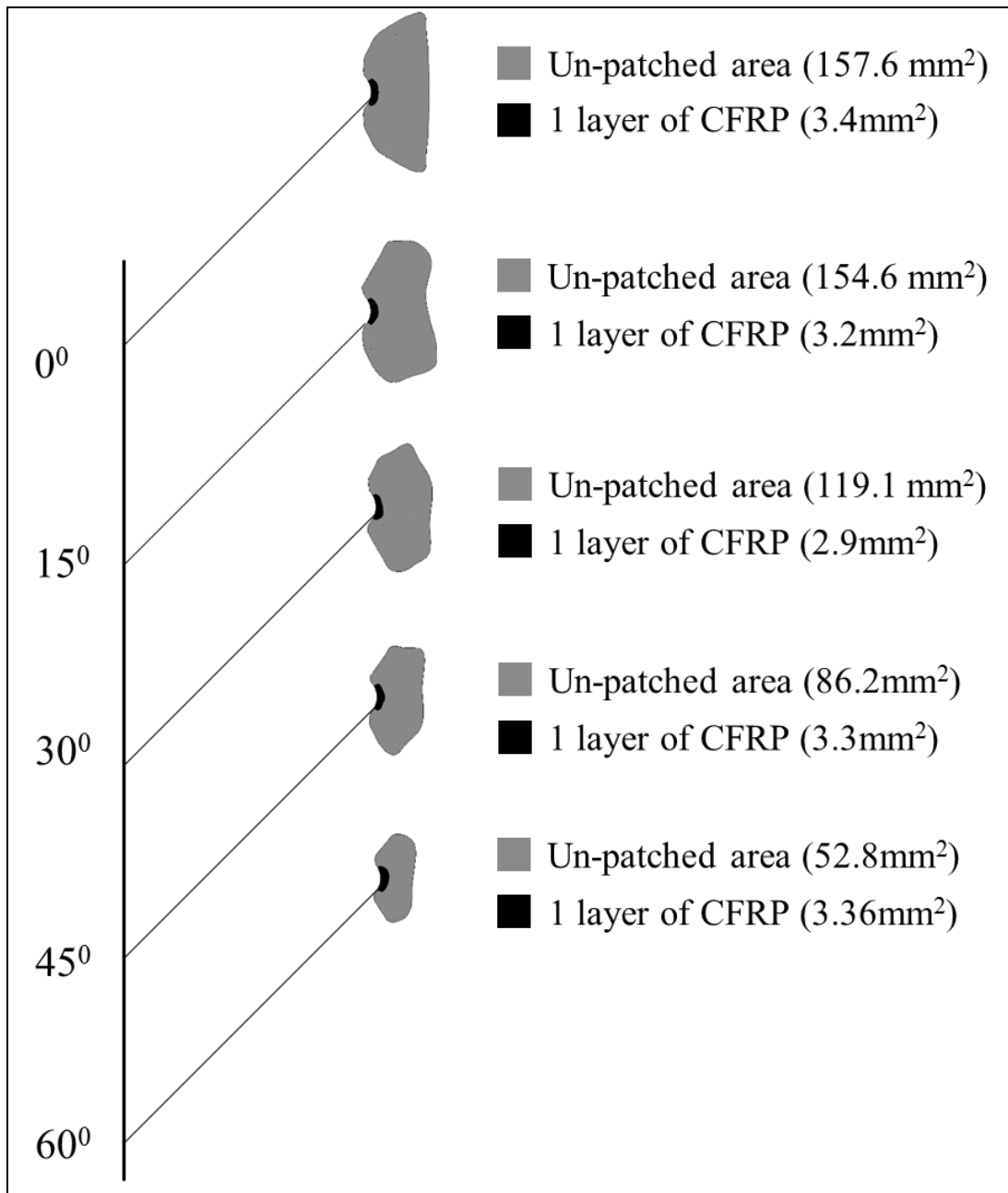


(a)

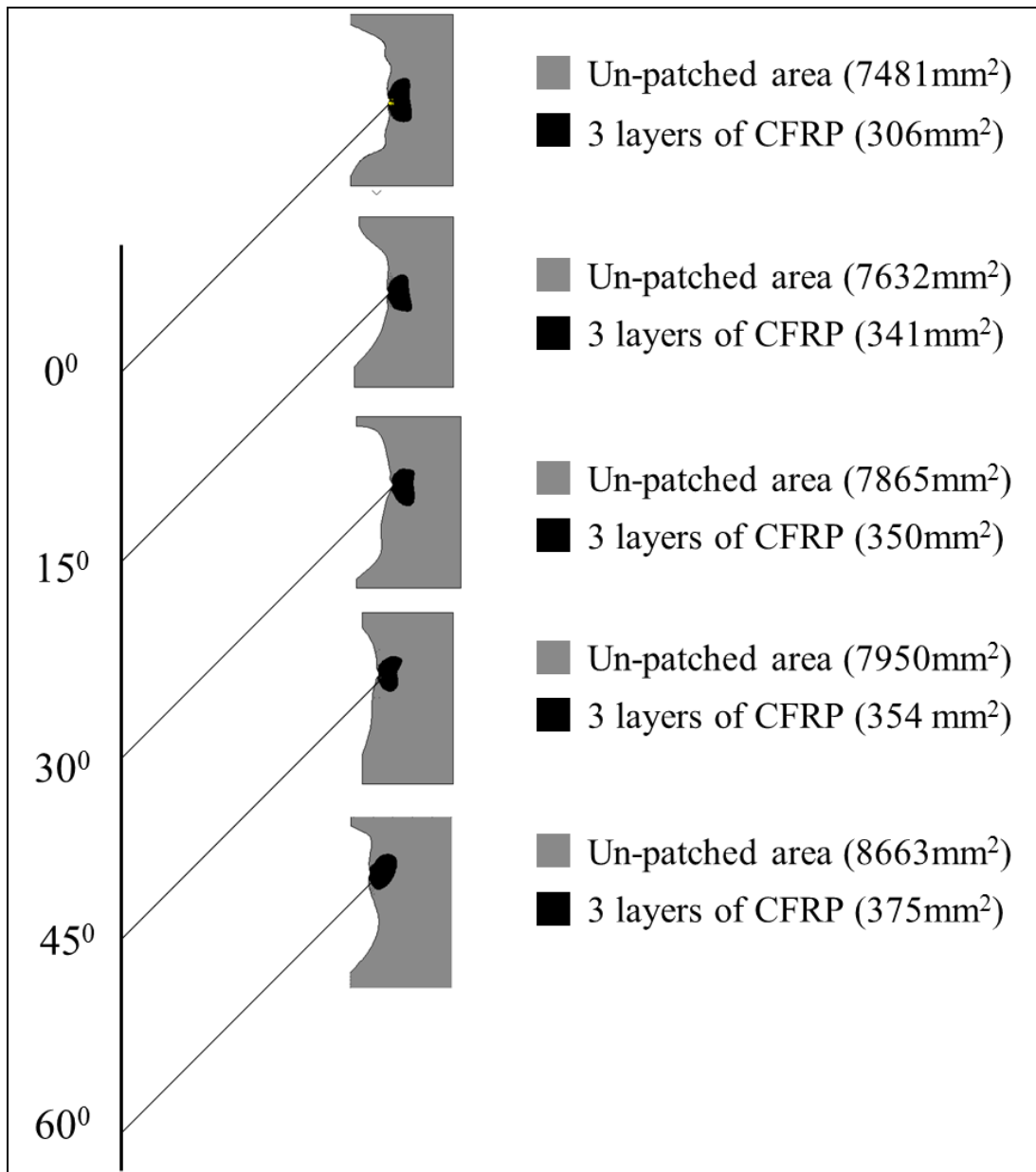


(b)

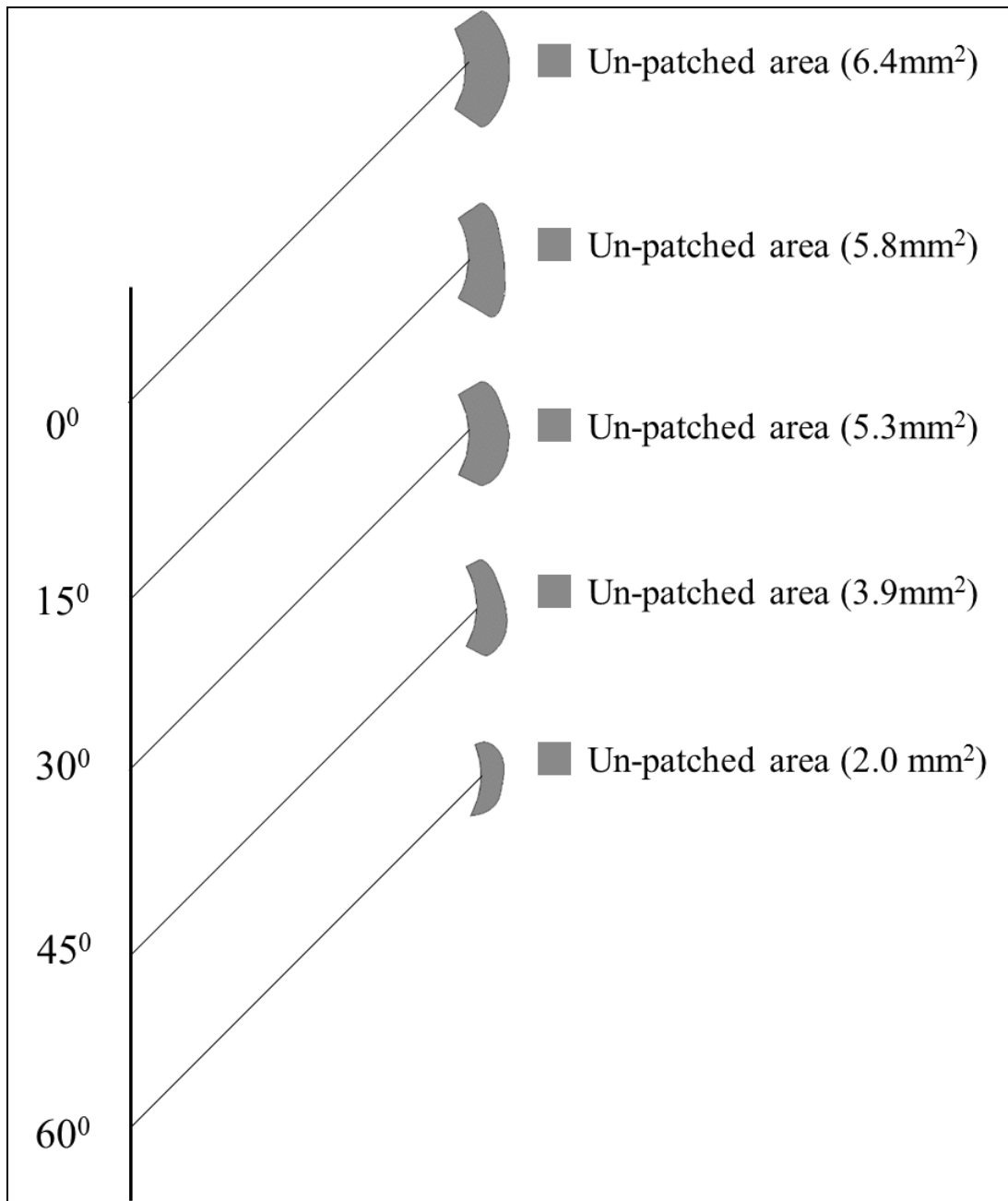
Figure 1(a) and 1(b): Meshing around the crack stop hole



**Figure 2: 25% Yield areas subjected to 41.2 MPa for various inclinations**

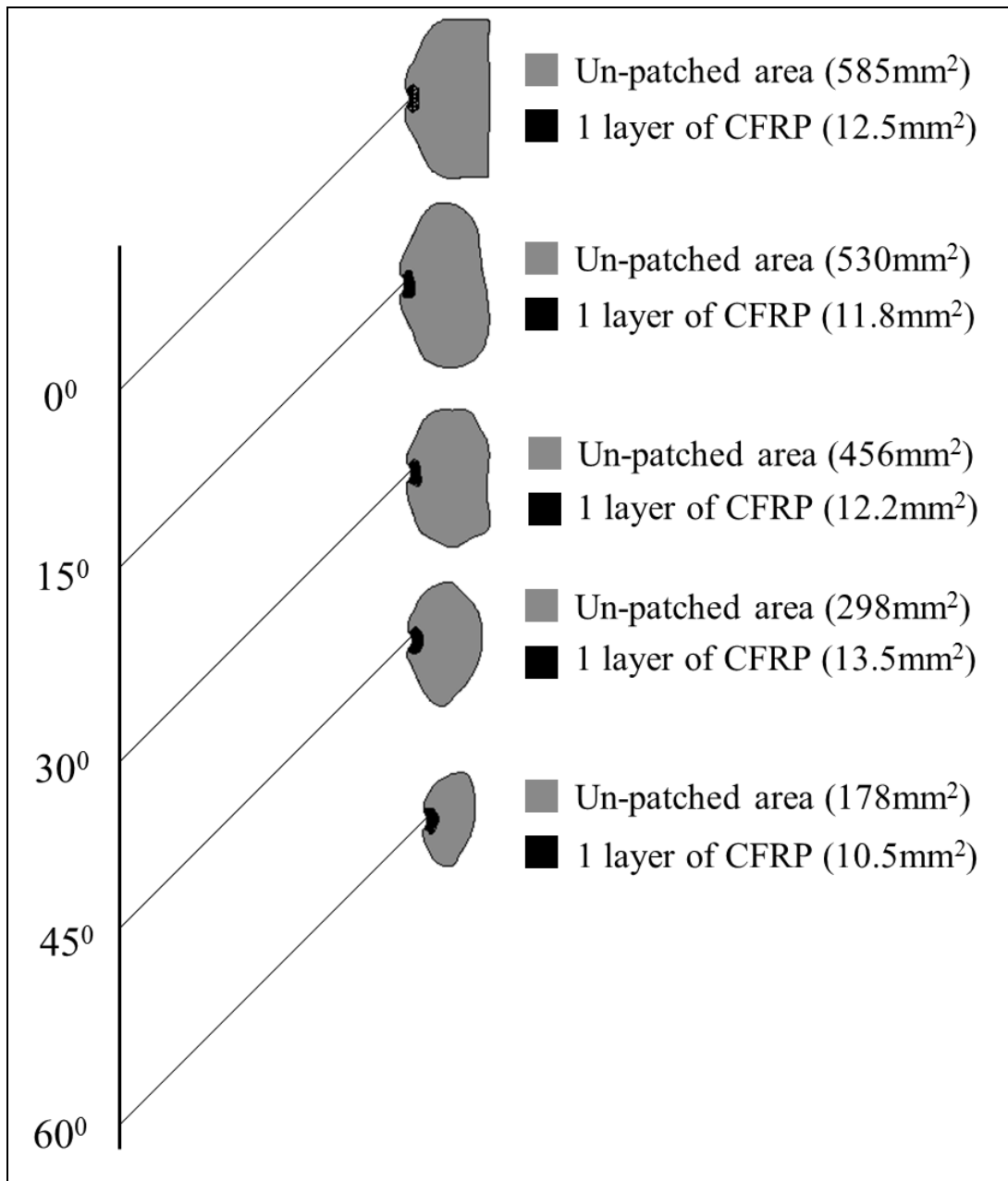


**Figure 3: 25% Yield areas subjected to 103.4 MPa for various inclinations**

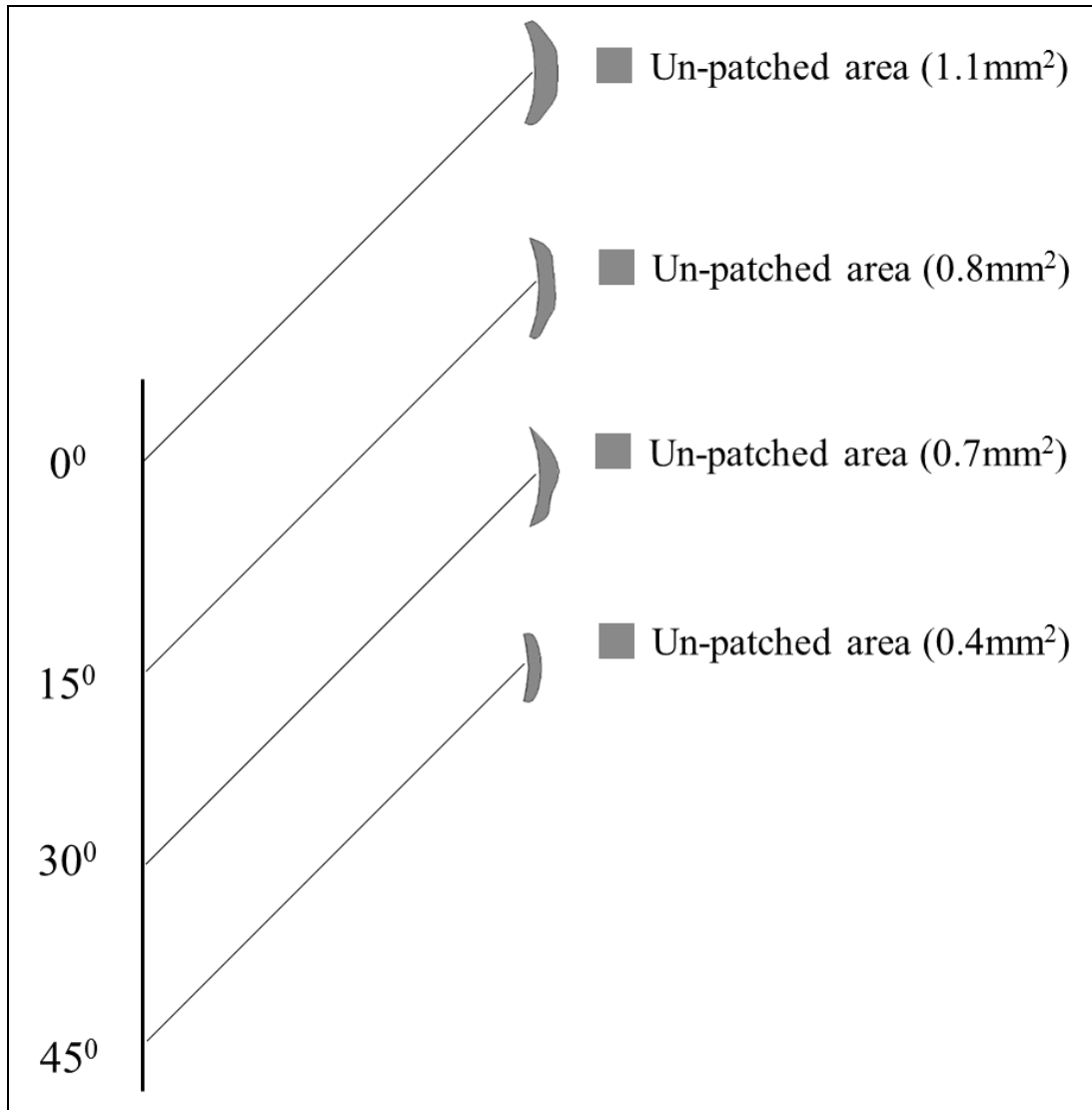


**Figure 4: 50% Yield areas subjected to 41.2 MPa for various inclinations**

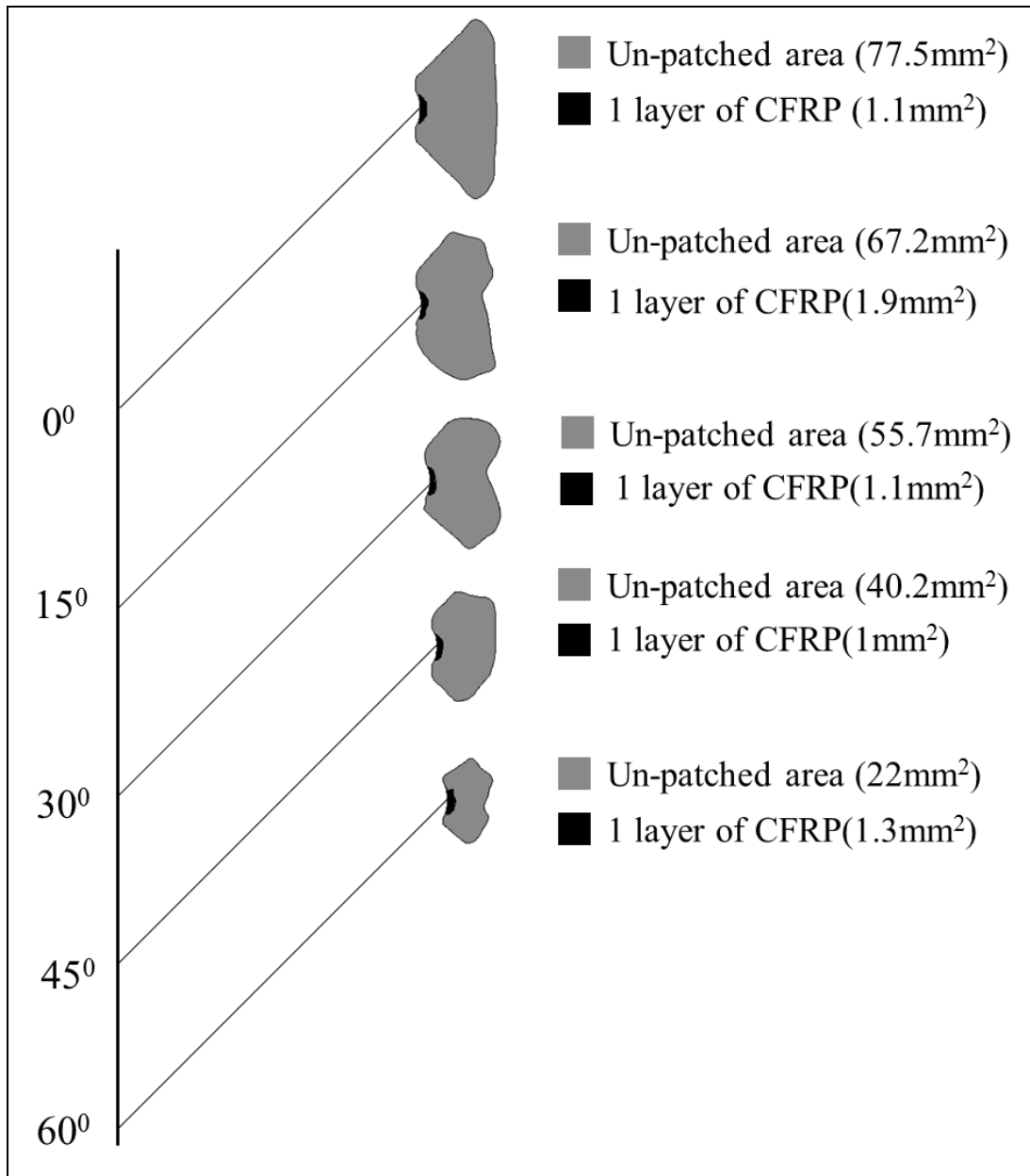












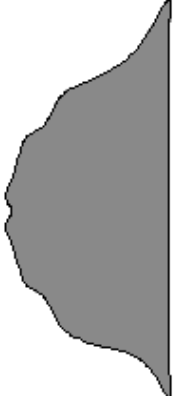


**Figure 4: 50% Yield areas subjected to 103.4 MPa for various inclinations**













**Figure 6: 75% Yield areas subjected to 41.2 MPa for various inclinations**










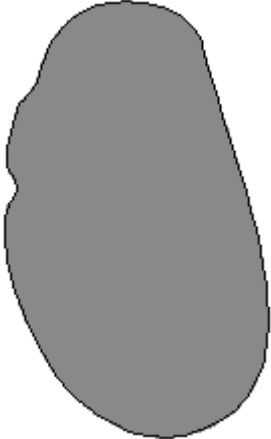


**Figure 7: 75% Yield areas subjected to 103.4 MPa for various inclinations**

|                     | 25% Yield<br>(>75Mpa)  | 50% yield<br>(>150Mpa)   | 75% Yield<br>(>225Mpa)   |
|---------------------|--|--|--|
| 7 Layer             | 0.06      |  |  |
| 6 Layer             | 0.22      |  |  |
| 5 Layer             | 0.68      |  |  |
| 4 Layer             | 1.38      |  |  |
| 3 layer             | 5.09      |  |  |
| 2 Layer             | 8.68     |  |  |
| 1 layer             | 41.86   | 0.57  |  |
| Bare Steel Specimen | 3621.8  | 46.3  | 7.16  |







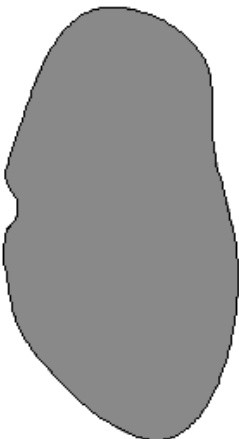


**Figure 8: Areas of 0 degree crack subjected to 62MPa load (all are in mm<sup>2</sup>)**

|                     | 25% Yield   | 50% yield  | 75% Yield  |
|---------------------|---|--|--|
| 6 Layer             | 0.23       |  |  |
| 5 Layer             | 0.56       |  |  |
| 4 Layer             | 2.0        |  |  |
| 3 layer             | 2.74       |  |  |
| 2 Layer             | 7.84       |  |  |
| 1 layer             | 40.1      | 0.42    |  |
| Bare Steel Specimen | 3703.55  | 39.22  | 7.11  |







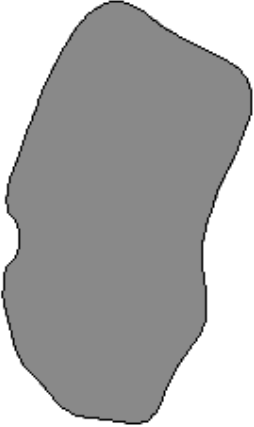


**Figure 9: Areas of 15 degree crack subjected to 62MPa load (all are in mm<sup>2</sup>)**

|                     | 25% Yield<br>(>75Mpa)  | 50% yield<br>(>150Mpa)   | 75% Yield<br>(>225Mpa)   |
|---------------------|--|--|--|
| 6 Layer             | 0.16      |  |  |
| 5 Layer             | 0.53      |  |  |
| 4 Layer             | 1.26      |  |  |
| 3 layer             | 2.64      |  |  |
| 2 Layer             | 6.95      |  |  |
| 1 layer             | 44.4    | 0.41    |  |
| Bare Steel Specimen | 2601.2  | 35.02  | 5.72  |

**Figure 10: Areas of 30 degree crack subjected to 62MPa load (all are in mm<sup>2</sup>)**




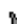








|                     | 25% Yield<br>(>75Mpa)   | 50% yield<br>(>150Mpa)   | 75% Yield<br>(>225Mpa)   |
|---------------------|---|--|--|
| 5 Layer             | 0.55       |  |  |
| 4 Layer             | 1.12       |  |  |
| 3 layer             | 3.36       |  |  |
| 2 Layer             | 7.51       |  |  |
| 1 layer             | 46.55     | 0.53    |  |
| Bare Steel Specimen | 1025.32  | 25.47  | 4.67  |

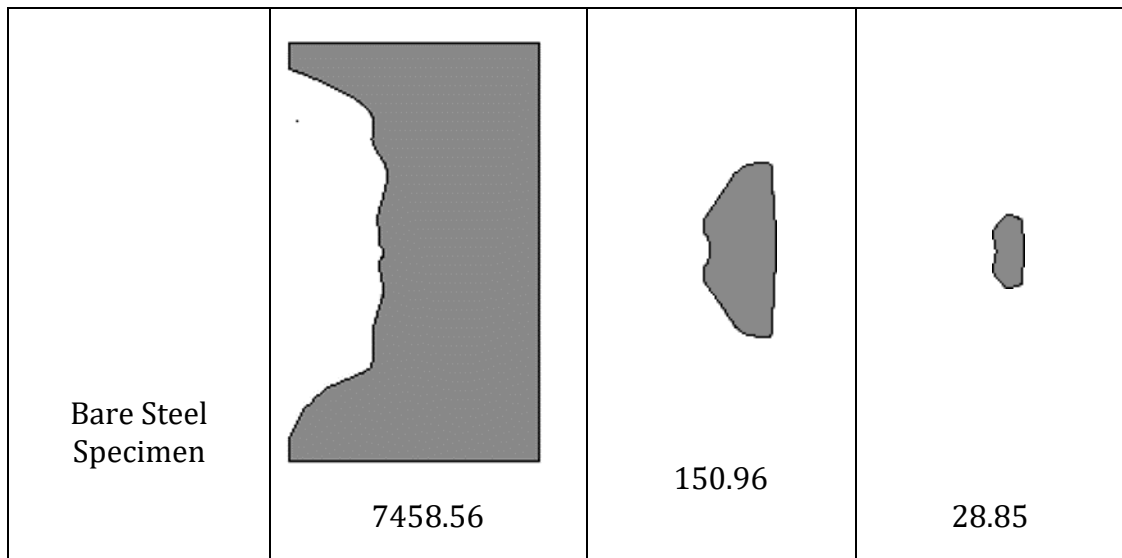
**Figure 11: Areas of 45 degree crack subjected to 62MPa load (all are in mm<sup>2</sup>)**

|                     | 25% Yield<br>(>75Mpa)   | 50% yield<br>(>150Mpa)  | 75% Yield<br>(>225Mpa)  |
|---------------------|---|---|---|
| 5 Layer             | 0.97         |   |   |
| 4 Layer             | 1.52         |   |   |
| 3 layer             | 3.31         |   |   |
| 2 Layer             | 9.49         |   |   |
| 1 layer             | <br>44.19   | <br>0.59   |   |
| Bare Steel Specimen | <br>594.24 | <br>12.48 | <br>2.26 |








**Figure 12: Areas of 60 degree crack subjected to 62MPa load (all are in mm<sup>2</sup>)**


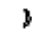


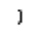





|         | 25% Yield<br>(>75Mpa)  | 50% yield<br>(>150Mpa)  | 75% Yield<br>(>225Mpa)  |
|---------|--|---|---|
| 8 Layer | 0.69          |   |   |
| 7 Layer | 1.19          |   |   |
| 6 Layer | 1.91          |   |   |
| 5 Layer | 3.66          |   |   |
| 4 Layer | 6.41          |   |   |
| 3 layer | <br>23.89     | 0.13       |   |
| 2 Layer | 86.81       | <br>0.71 |   |
| 1 layer | <br>1637.58 | <br>3.46 | <br>0.15 |















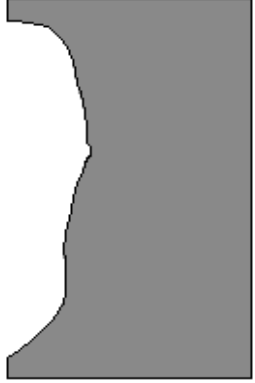


**Figure 13: Areas of 0 degree crack subjected to 82.7MPa load (all are in mm<sup>2</sup>)**

|         | 25% Yield (>75Mpa)   | 50% yield (>150Mpa)   | 75% Yield (>225Mpa) |
|---------|--|---|---------------------|
| 8 Layer | 0.68      |   |                     |
| 7 Layer | 1.2       |   |                     |
| 6 Layer | 2.05      |   |                     |
| 5 Layer | 3.49      |   |                     |
| 4 Layer | 5.73      |   |                     |
| 3 layer | <br>20.13 | <br>0.11 |                     |



|                     |   |  |   |
|---------------------|---|--|---|
| 2 Layer             | <br>79.63    | <br>0.66    |   |
| 1 layer             | <br>1772.43  | <br>3.29    | <br>0.13 |
| Bare Steel Specimen | <br>7410.60 | <br>152.77 | <br>25.0 |










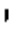
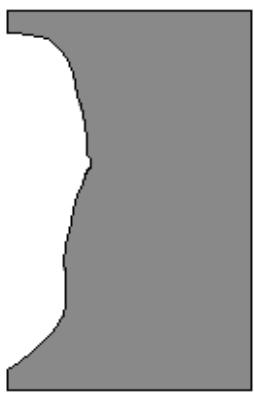


**Figure 14: Areas of 15 degree crack subjected to 82.7MPa load (all are in mm<sup>2</sup>)**

|         | 25% Yield<br>(>75Mpa)  | 50% yield<br>(>150Mpa) | 75% Yield<br>(>225Mpa) |
|---------|--|------------------------|------------------------|
| 8 Layer | 0.54  |                        |                        |
| 7 Layer | 1.02  |                        |                        |
| 6 Layer | 1.64  |                        |                        |
| 5 Layer | 3.1   |                        |                        |









|                     |  |  |   |
|---------------------|--|--|---|
| 4 Layer             | 6.11      |  |   |
| 3 layer             | 20.99     | 0.13      |   |
| 2 Layer             | 90.63     | 0.70      |   |
| 1 layer             | 1188.09   | 3.24      | 0.13     |
| Bare Steel Specimen | 7315.12  | 124.63  | 20.42  |




**Figure 15: Areas of 30 degree crack subjected to 82.7MPa load (all are in mm<sup>2</sup>)**

|         | 25% Yield<br>(>75Mpa)  | 50% yield<br>(>150Mpa) | 75% Yield<br>(>225Mpa) |
|---------|--|------------------------|------------------------|
| 8 Layer | 0.54  |                        |                        |
| 7 Layer | 1.02  |                        |                        |

|                     |   |  |   |
|---------------------|---|--|---|
| 6 Layer             | 1.64       |  |   |
| 5 Layer             | 3.1        |  |   |
| 4 Layer             | 6.11       |  |   |
| 3 layer             | 20.99      | 0.13      |   |
| 2 Layer             | 90.63      | 0.70      |   |
| 1 layer             | 1188.09   | 3.24    | 0.13   |
| Bare Steel Specimen | 7315.12  | 124.63  | 20.42  |

**Figure 16: Areas of 45 degree crack subjected to 82.7MPa load (all are in mm<sup>2</sup>)**

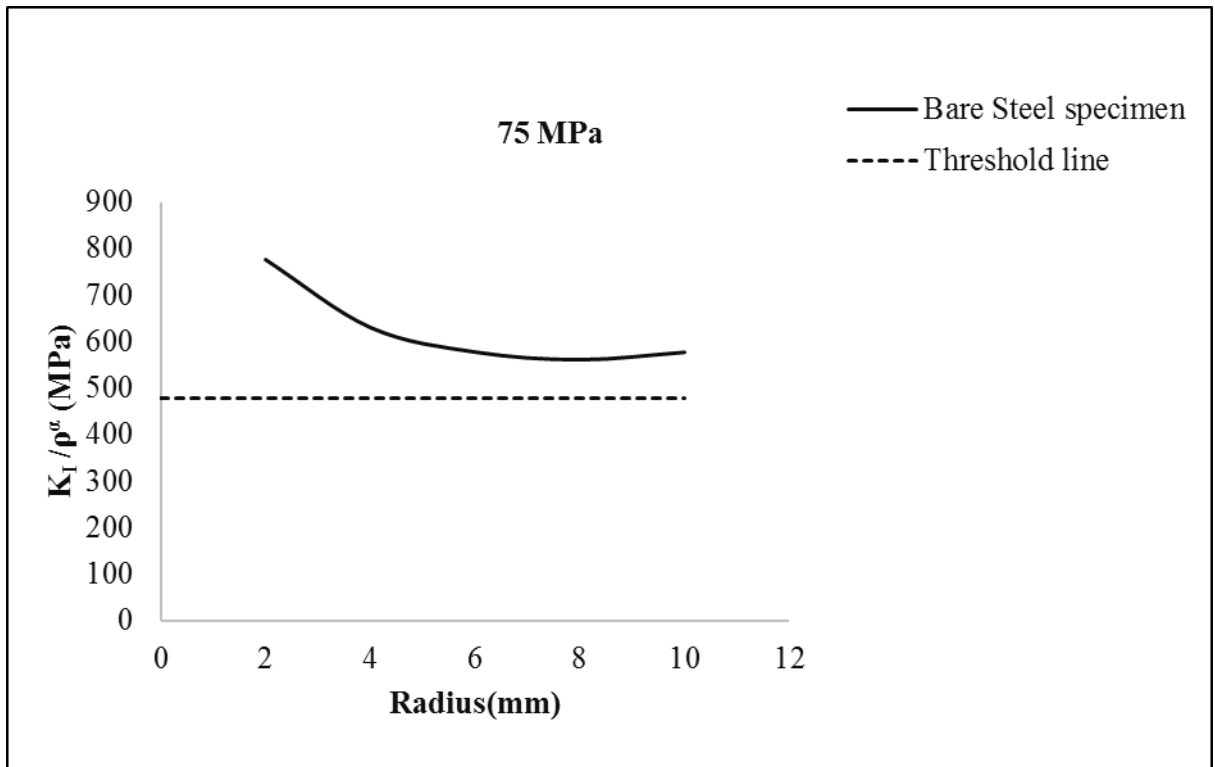
|         | 25% Yield<br>(>75Mpa)  | 50% yield<br>(>150Mpa) | 75% Yield<br>(>225Mpa) |
|---------|--|------------------------|------------------------|
| 8 Layer | 1.06      |                        |                        |
| 7 Layer | 1.52      |                        |                        |
| 6 Layer | 2.37      |                        |                        |
| 5 Layer | 3.91      |                        |                        |
| 4 Layer | 8.76    |                        |                        |
| 3 layer |  26.17  | '<br>0.12              |                        |
| 2 Layer | 98.77   | '<br>0.86              |                        |
| 1 layer |  825.98 | '<br>3.60              | '<br>0.15              |

|                     |   |   |   |
|---------------------|---|---|---|
| Bare Steel Specimen |  |  |  |
|                     | 7257.04   | 54.96   | 7.89  |

**Figure 17: Areas of 60 degree crack subjected to 82.7MPa load (all are in mm<sup>2</sup>)**

| Coefficient<br>s | Coefficients |        |        |        |      |
|------------------|--------------|--------|--------|--------|------|
|                  | a            | b      | C      | d      | E    |
| <b>p0</b>        | -111         | 296    | -288   | 123    | -22  |
| <b>p1</b>        | 866          | -2280  | 2174   | -894   | 139  |
| <b>p2</b>        | 143          | -380   | 366    | -154   | 25   |
| <b>p3</b>        | -1798        | 4699   | -4425  | 1782   | -266 |
| <b>p4</b>        | 783          | -2105  | 2064   | -882   | 144  |
| <b>p5</b>        | -3005        | 7978   | -7702  | 3237   | -525 |
| <b>p6</b>        | 11390        | -29943 | 28460  | -11648 | 1794 |
| <b>p7</b>        | -5886        | 15336  | -14368 | 5729   | -836 |
| <b>p8</b>        | 898          | -2241  | 1969   | -707   | 85   |

**Figure 18: Variation of p0 to p8 with coefficients a, b, c, d and e**



**Figure 19: Calculation of optimum crack stop hole radius**



# Chapter 2

## Effect of crack stop hole and asymmetrically bonded CFRP layers on yielded areas of steel plate

### 2.1 Introduction

Due to fatigue loads cracks may initiate in structural members which will increase the stress near the crack tip leads to further propagation of crack. Stress intensity factor (K) is the term used to measure the effect of crack and  $K_I$ ,  $K_{II}$  and  $K_{III}$  are three different types of stress intensity factors which depend on the relation between the directions of load applied, crack front and crack propagation. In the present study, only  $K_I$  corresponding to mode I is considered because when inclined cracks are subjected to mixed mode of cracking but due to the presence of crack stop hole it will end up in mode I cracking which is shown in fig. 3. To repair this type of cracks, there are several types of retro fitting techniques crack stop holes, peening, Gas Tungsten Arc (GTA) welding and strengthening with steel plate or CFRP laminates. Among these crack stop hole repair technique has more effect in reducing the SIF at the crack tip which is the main objective of any retrofitting technique.

The expression for SIF ( $K_I$ ) (Eq. 1) was first provided by Irwin for specimen shown in Fig. 1a, later proposed an expression of  $K_I$  for a specimen shown in Fig. 1b.

$$K_I = \sigma_{applied} * \sqrt{\pi a} \quad (1)$$

$$K_I = \frac{\sigma_{y max} * \sqrt{\pi \rho}}{2} \quad (2)$$

The expressions (Eqs.3, 4 & 5) represent the stress state at the edge of the notch obtained by shifting the origin to a distance half of the radius ( $\rho/2$ ) behind the crack front.

$$= \frac{K_I}{\sqrt{2\pi r}} \cos \frac{\theta}{2} \left( 1 - \sin \frac{\theta}{2} \sin \frac{3\theta}{2} \right) - \frac{K_I}{\sqrt{2\pi r}} \frac{\rho}{2r} \cos \frac{3\theta}{2} \quad (3)$$

$$= \frac{K_I}{\sqrt{2\pi r}} \cos \frac{\theta}{2} \left( 1 - \sin \frac{\theta}{2} \sin \frac{3\theta}{2} \right) + \frac{K_I}{\sqrt{2\pi r}} \frac{\rho}{2r} \cos \frac{3\theta}{2} \quad (4)$$

$$= \frac{K_I}{\sqrt{2\pi r}} \cos \frac{\theta}{2} \left( \sin \frac{\theta}{2} \sin \frac{3\theta}{2} \right) - \frac{K_I}{\sqrt{2\pi r}} \frac{\rho}{2r} \sin \frac{3\theta}{2} \quad (5)$$

The relationship between two terms,  $K_I / \sqrt{\rho}$  and maximum stress at the edge of the hole ( $\sigma_{y \max}$ ) given in (Eq. 2) by Creagor and Paris has been derived based on LEFM concepts i.e. by substituting  $r=\rho/2$  and  $\Theta=0$  in Eq. 4.

If yielding of material is allowed maximum stress a head of the crack stop hole remains constant for a distance of  $X_c$  which is known as characteristic distance and by substituting  $\theta = 0$  and  $r = X_c + \frac{\rho}{2}$  in Eq. 4 and we get Eq. 6 after rearranging the terms as shown below.

$$\sigma_y = \frac{K_I}{(2\pi(X_c + \frac{\rho}{2}))^{\frac{1}{2}}} \left[ 1 + \frac{\rho}{2(X_c + \frac{\rho}{2})} \right]$$

$$\sigma_y = \frac{K_I}{(2\pi(X_c + \frac{\rho}{2}))^{\frac{1}{2}}} \left[ \frac{2X_c + \rho + \rho}{2(X_c + \frac{\rho}{2})} \right]$$

$$\sigma_y = \frac{K_I}{(2\pi(X_c + \frac{\rho}{2}))^{\frac{1}{2}}} \left[ \frac{2(X_c + \rho)}{2(X_c + \frac{\rho}{2})} \right]$$

$$\sigma_y = \frac{K_I}{(2\pi)^{\frac{1}{2}}} \cdot \frac{(X_c + \rho)}{(X_c + \frac{\rho}{2})^{3/2}}$$

$$K_I = \sigma_y (2\pi)^{\frac{1}{2}} \frac{(X_c + \frac{\rho}{2})^{3/2}}{(X_c + \rho)} \quad (6)$$

From experimental studies of Boukharouba (2004) has given an another expression of  $K_I$  (Eq. 7) for a crack with crack stop hole which is a function of characteristic distance ( $X_c$ ) and stress gradient ( $\alpha$ ).

$$K_p = \sigma_{yy}(X_c) * \sqrt{2\pi} \left( X_c + \frac{\rho}{2} \right)^\alpha \quad (7)$$

To get the optimum hole radius to arrest the crack propagation, Barsom (2004) proposed an a threshold value shown in Eq. 8 and shown in Fig. 6.

$$\frac{K_I}{\sqrt{\rho}} = 10\sqrt{\sigma_{ys}} \quad (8)$$

But due to geometrical and site restrictions it may not be possible to drill an adequate size of crack stop hole which will create an undersized hole leads to

reinitiation of crack. To improve the repair efficiency and to arrest the crack propagation a combination of crack stop hole and CFRP on structural members has to be studied. In the present study, asymmetrically bonded CFRP case is considered because to simulate the situations like inaccessibility of the other side of the member.

## **2.2 Background**

Inglis (1913) worked mathematically on the stresses in a plate due to cracks and sharp corners. Mainly worked on the determination of stresses around a hole (elliptic in form) in a plate. Concluded that, in case of brittle materials a fine scratch on the surface produces a local weakness which can create a fracture due to applied forces along the line of the scratch. In case of ductile materials, local stresses at the end of crack will be effected by plastic yield. A small alternating load may produce an alternating stress far in excess of its elastic range. No amount of ductility can stop the crack propagation if crack is fairly started. Arendt and Sun (1994) worked on bending effects of unsymmetric adhesively bonded composite repairs on cracked aluminium panels. By using modified crack closure method stress intensity factors and strain energy release rates were obtained. Concluded that the Total strain energy release rate is directly proportional to adhesive thickness and inversely proportional to shear modulus and stiffness. Unsymmetric repair causes crack growth instability, but relatively better than unrepaired crack. Variation of stress intensity factor is negligible over the thickness of cracked plate.

Naboulsi and Mall (1996) worked on the repair of cracked metallic structure using an adhesively bonded composite patch using the three-layer technique (which is

capable of investigating the adhesive effects in depth) in two-dimension finite element analysis. The results from the study are: debond growth in single sided repair is larger than the double sided repair, effect of cohesive crack (crack in the plate) on debond is local and adhesive crack (debond) is driven due to cohesive crack growth. Finally the three layer technique is an accurate alternative model for investigating repair of cracked metallic structure. Turaga et al. (1999) worked on modelling of a patch repair to a thin cracked metallic sheets. Compares the outcome of different finite element modelling strategies. To study the effect of patch material, patch size, patch symmetry and adhesive thickness on repair performance, the established and efficient finite element modelling approach is used. For accurate analysis of single sided patch repair, single brick across the thickness of sheet, adhesive and patch is enough on three-dimensional geometrical non-linear finite element analysis.

Shankar and Wu (2001) worked experimentally on fatigue behaviour of welded 5083-H321 aluminium alloy plates when weld-repair technique is employed, by three-dimensional finite-element analysis stress intensity factors for cracks in the weld line and crack closure effects of weld residual stresses were evaluated. Found that when cracks in the weld reinforcement are repaired by welding only on one side, the crack growth rates of the repaired specimens are quite similar in magnitude to those of the as-welded plates and the parent material. Concluded that the weld repair technique is a poor means of enhancing fatigue life. Seo and Lee (2002) investigated the fatigue crack growth behaviour of cracked thick aluminium plate repaired with bonded composite patch. Stress intensity factor of crack and fatigue life determined from experimental result was compared with 3D Finite element

analysis results. Results have shown that the stress intensity factor of thick specimen showed a large variation through thickness direction.

Chung and Wang (2003) studied experimentally the fatigue crack growth behaviour of aluminium plates reinforced with composite material patch on one side with five ( $0^\circ$ ,  $15^\circ$ ,  $30^\circ$ ,  $45^\circ$  and  $60^\circ$ ) different crack inclinations. The results indicate that the fatigue life of patched plate with inclined crack increased approximately 2.4-5.0 times compared to no-patched plate. Shaat et al. (2004) describes the research progress in strengthening and repair of steel structures by using fiber reinforced polymers. Explained about retrofit of naturally deteriorated steel girders, repair of notched girders, strengthening of undamaged girders, repair of steel girders acting compositely with a concrete deck, fatigue behaviour of steel sections retrofitted with FRP and retrofit of tubular steel sections. Application of CFRP increases the moment capacity, strength, stiffness, yielding load and fatigue life of the structure. Bonding the FRP reinforcement to the compression side should be effective. A nonconductive layer between the FRP and steel should be provided to resist galvanic corrosion. Thicker the reinforcing material, higher the chance of bond failure. These are some of the guidelines to use FRP on steel structures.

Tsai and Shen (2004) worked on stress intensity factor analysis and the fatigue life calculations are performed for the cracked aluminium plate and the cracked plate repaired with the composite patches. Concluded that the stress variation in thickness direction did not maintain the same route for different crack lengths. For single-side repaired aluminium plate, the biggest stress intensity factor was obtained at the front side or composite patching side.

Hossein et al. (2006a) and (2006b) developed a procedure to obtain the crack trajectories using dynamic mesh generation for single-sided repaired panels in both mode I and mixed mode conditions. The results indicate that the fatigue crack growth life obtained from the developed procedure is compatible with the experimental results for mode I conditions and non-conservative in some cases. The results also indicate that while the J-integral values at the mid-plane of the cracked plates reduce with increasing patch thickness for both mode-I and mixed-mode crack loading conditions, it does not have considerable effect on the crack propagation path. Worked experimentally and numerically on fatigue crack propagation of single side repaired centrally cracked aluminium panels. Worked on the parameters influencing stress intensity factor, crack growth rate and effect of crack-front shape on fatigue crack growth in mode-I condition of a single side repaired panel. Developed a simple method to predict the crack growth life of single side repaired aluminium panels. Concluded that the single-side repair of thin panels using glass/epoxy composite patch is more efficient than the thick panels.

Liu et al. (2009) (a), (b) and (c) worked on calculating stress intensity factors, crack propagation and fatigue life by using boundary element analysis in the numerical software program BEASY. Evaluated the influence of bond length, bond width, patch configuration, CFRP layer number, the modulus of the composite patch and adhesive shear modulus on the stress intensity factors and their fatigue lives. Studied experimentally on fatigue crack propagation and fatigue life of steel plates when CFRP sheet is adopted on both single side and double side of the plate. Patch thickness, patch length and patch configuration have slightly more influence on single-sided repairs than on double-sided repairs. Observed that normal modulus

CFRP, had failed by debonding and high modulus CFRP failed by fibre breakage. Worked theoretically to develop an analytical model for both developed for both double-sided and single-sided repairs. Studied with two of fibre sheets one is normal modulus CFRP and another is high modulus CFRP. Single sided configuration induces out-of-plane bending which increases the stress intensity factor at crack tip. Assumed that effect of crack closure and out-of- plane bending on the stress intensity factor are counteracted. Finally concluded that, efficiency of increasing fatigue life is not significant by single-sided repair.

Hosseini et al. (2013) Investigated on effects of patch material, patch width, patch thickness, adhesive thickness, and bonding shear strength on progressive damage of bonding on composite patch under static and cyclic loading using cohesive elements. Concluded that the smaller values for elastic modulus of patch, patch thickness and adhesive thickness and also larger values of adhesive shear strength and patch width are more desirable. Sourabh et al. (2014) studied on the compression behaviour of the of an open hole compression behaviour of an open-hole Carbon fiber reinforced plastic (CFRP) panel adhesively bonded with the external CFRP patch to predict the damage mechanism of CFRP panel by using stress-based 3D-Hashins failure criteria along with Yes delamination criteria. Found a good coherence between Finite element based 3D progressive damage model and experimental predictions. Concluded that Final failure in repaired panels are observed due to the shear failure in the adhesive layer that to after complete debonding of patch in which patch debonding initiates from the patch overlap edge. Suzuki experimentally studied on repair of cracked steel member by CFRP strip and stop-hole. The three types of specimen used in study are (i) Repair by stop holes only (ii) Repair by both stop



holes and the CFRP strip with 10mmx1.2mmx100mm and (iii) Repair by both stop holes and the CFRP strip with 25mmx1.2mmx100mm. Concluded that the efficiency of repair increases as width of the CFRP strip increases and a ratio (width of CFRP strip to crack length) of 0.4 is enough to provide a first-aid repair.

Kashfuddoja and Ramji (2015) experimentally worked on the optimum overlap length in patch design for the repair of single sided (unsymmetrical) CFRP patch and also closely monitored the failure mechanism, load displacement behaviour, damage initiation and propagation by using Digital image correlation (DIC) technique and a methodology is demonstrated the full field through the thickness strain measurement in a thin adhesive layer by employing the DIC technique. They recommended to have minimum/optimum overlap length in the range of 1.5–2 times the cut-out diameter. Srilakshmi et al. (2015) worked on the fatigue life of unrepaired and repaired Al-2014-T6 panels with an inclined center crack in which panels are repaired through single-sided and double-sided adhesively bonded carbon fiber reinforced polymer (CFRP) patch. Concluded that, for single sided patch repair configuration there is a marginal increase in  $K_{II}$  with the increase in crack length and fatigue life of both the single- and double-sided patch repaired panels, are higher than the unrepaired panel and in the single-sided repaired panels, non-uniform crack growth is observed.

### **2.3 Geometry and FE modelling**

The specimen geometry is taken from the experimental work of Barsom and Nicol (1974) and modified from double edge notch specimen to central crack specimen to model the effect of crack stop hole. The magnitudes of loads applied are 41.2 MPa

(6 ksi), 62 MPa (9 ksi), 82.7 MPa (12 ksi), 103.4 MPa (15 ksi) which were reported as loads that the bridge girders are generally subjected to (Fisher, 1980). The connection between CFRP, steel plate and CFRP, adhesive is modeled using bonded contact. In bonded contact, contacting surfaces are assumed to be glued together throughout the analysis. To create bonded contact, contact and target elements need to be defined on the faces of elements, where they come into contact. In this study, multipoint constraint (MPC) algorithm is used for bonded contact. CFRP laminate is modeled as an orthotropic material. The CFRP material properties are taken from Ramji et al (2013) and in the present study, the number of CFRP layers varied are 10 which range from 0 to 10 numbers. The thickness of the lamina reported in the reference is 0.375mm and CFRP patch length ( $l$ ) is taken as 127 mm based on the numerical study by Zhao and Zhang (2007).

Incremental meshing as given by Nakamura and Parks (1989) is employed around the hole to capture the sharp stress gradient because the value of stress at the edge of the hole is sensitive to element size. The number of elements used around the hole is 6 elements in thickness direction shown in Fig. 1 and 20 elements in radial direction and 48 elements in angular direction as shown in Fig. 1. Although the applied loads are less than the yield stress of steel, localized yielding occurs at crack tip. Therefore, to take into account the local yielding behavior, a nonlinear Finite Element Analysis (FEA) is carried out in this research work using ANSYS 12.0 software. The material model used for Steel is Multi Linear Isotropic hardening. For modeling all components (i.e. steel plate, adhesive, and CFRP plate) Solid 186

element is used. Solid 186 element has mid side nodes and it performs better in stress singularity regions and for nonlinear analysis.

## **2.4 Results and discussion**

### **2.4.1 Effect of crack stop hole and CFRP layers on yielded areas of Steel plate:**

The present study is focused on studying the effect of combination of crack stop hole and CFRP patches to arrest the crack propagation, in which single sided repair is considered. After running analysis, calculated the area which is greater than the 25% yield (>75MPa), 50% yield (>150MPa) and 75% yield (>225MPa) when plate is subjected to four different loads 41.2MPa, 62MPa, 82.7MPa and 103.4MPa for various crack inclinations  $0^0$ ,  $15^0$ ,  $45^0$  and  $60^0$ . On capturing the position of nodes, plotted in AUTOCAD 2012 to find the exact area of stressed regions.

The results have shown that, on patched side the stressed areas on steel plate will be decreasing on increasing the number of layers, but from one particular layer area starts increasing which is due to bending effect. The bending effect is due to asymmetry of axial stiffness. This bending results in compression on patched side and tension on patched side. On patched side the areas of stressed regions are small compared to unpatched side. The areas with stressed regions are explained briefly in Fig. 2,3,4 and 5

The results have shown that the combination of crack stop hole and CFRP patch effectively arrest the crack propagation

## 2.5 Calculation of crack stop hole radii and number of CFRP layers required to stop the crack propagation

### 2.5.1 Example 1

Consider a load of 34.4 MPa (5 ksi) acting on a specimen with center crack of length 2". The steel and CFRP properties and dimensions are the same as considered in this paper. The site conditions are such that the maximum radius of hole that can be drilled is 4mm. Determine the number of CFRP layers required to arrest the crack.

Solution: The solution to the problem is carried out in a step by step format as shown below: 1. Calculate  $K_I / \sqrt{\rho}$  of a bare steel specimen and plot the variation of the same with respect to various crack stop hole radii (0.375" to 1/32") as shown in Fig. 7

$$K_{\rho} = \sigma_{yy}(X_c) * \sqrt{2\pi} \left( X_c + \frac{\rho}{2} \right)^{\alpha}$$

2. Plot the threshold line given by Barsom equation shown below in the same plot of  $K_I / \sqrt{\rho}$  versus crack stop hole radii to determine the threshold radius. The threshold radius in this case is 6mm which is greater than the 4mm hole that can be drilled at site necessitating the need to reinforce the crack with CFRP patch to prevent crack re-initiation.

$$\frac{K_I}{\sqrt{\rho}} = 10\sqrt{\sigma_{ys}}$$

3. Now, as a start assume that 1 layer of CFRP patch is required with a crack stop hole radii of 3 mm.

4. Input the parameters 2a (50.8 mm),  $\rho$  (3 mm) and  $\sigma_{\text{applied}}$  (34.4 MPa) in equation shown below and determine coefficients a through e by using corresponding p0 through p16 for each coefficient using Fig. 6

$$p0 + p1 * x + p2 * y + p3 * x^2 + p4 * y^2 + p5 * x * y + p6 * x^2 * y + p7 * x * y^2 + p8 * y^3$$

5. Using the coefficients a through e obtained from Step 4 and SR from Eq. 6, calculate RF using equation shown below. The RF value comes to around 0.391.

$$\text{Reduction factor} = \frac{(K_I / \rho^\alpha)_{\text{with CFRP}}}{(K_I / \rho^\alpha)_{\text{w/o CFRP}}}$$

$$RF = a (SR^5) + b (SR^4) + c (SR^3) + d (SR^2) + e (SR) + 1$$

6. From Fig. 7, the value of  $K_I / \rho^\alpha$  of a bare steel specimen with crack stop hole radius of 3 mm is approximately 600 MPa. The corresponding value of specimen reinforced with 1 CFRP layer will be 234.6 MPa (0.391\*600).

7. The reduced  $K_I / \rho^\alpha$  value (234.6 MPa) is now compared with  $10\sqrt{\sigma_{ys}}$  (477 MPa). This value (477 MPa) is greater than reduced  $K_I / \rho^\alpha$  value (234.6 MPa) which indicates that 1 layer of CFRP with 3 mm radius will not result in crack re-initiation. Since the site conditions in the problem permit up to 4mm crack stop hole radius, the assumed 1 layer of CFRP reinforcement with 3 mm crack stop hole radius (undersized) is valid.

A nonlinear FEA carried out for the above conditions (2a= 50.8 mm,  $\rho$ = 3mm, SR = 0, 0.08, load = 34.4mm) and calculated  $K_I / \rho^\alpha$  for bare steel specimen and patched

specimen with 1 layer are respectively 591 MPa and 269 MPa, which indicate that the RF value is 1, 0.456 respectively. It can be observed that the difference is -14.6% between proposed equation and FEA indicating the accuracy of the proposed equation.

### 2.5.2 Example 2

Consider a load of 51.7 MPa (7.5 ksi) acting on a specimen with center crack of length (2a) 44.45 mm (1.75"). The steel and CFRP properties and dimensions are the same as considered in this paper. The site conditions are such that the maximum radius of hole that can be drilled is 10mm. Determine the number of CFRP layers required to arrest the crack.

Solution: The solution to the problem is carried out in a step by step format as shown below: 1. Fig. 8 is plotted based on steps 1 and 2 in Ex.1.

2. Unlike Ex.1, there is no intersection between the threshold line and the bare steel specimen curve obtained from FEA indicating that a CFRP patch is mandatory (crack stop hole alone is not enough) to reduce the SIF.

3. From the given conditions, as a start it is assumed that 1 layer of CFRP patch with a crack stop hole radii of 9.525 mm is required to arrest a crack.

4. Input the parameters 2a (44.45 mm),  $\rho$  (9.525 mm) and  $\sigma_{\text{applied}}$  (51.7 MPa) in equation shown below and determine coefficients a through e by using corresponding p0 through p16 for each coefficient using Fig. 6

$$p0 + p1 * x + p2 * y + p3 * x^2 + p4 * y^2 + p5 * x * y + p6 * x^2 * y + p7 * x * y^2 + p8 * y^3$$

5. Using the coefficients a through e obtained from Step 4 and SR from equation shown below, calculate RF using equation shown below. The RF value comes to around 0.5091.

$$RF = a (SR^5) + b (SR^4) + c (SR^3) + d (SR^2) + e (SR) + 1$$

6. From Fig. 8, the value of  $KI / \rho\alpha$  of a bare steel specimen with crack stop hole radius of 9.525 mm is approximately 577 MPa. The corresponding value of specimen reinforced with 1 CFRP layer will be 293.75 MPa ( $0.5091 \cdot 577$ ).

7. The reduced  $KI / \rho\alpha$  value (293.75 MPa) is now compared with  $10\sqrt{(\sigma_{ys})}$  (477 MPa). This value (477 MPa) is greater than reduced  $KI / \rho\alpha$  value (293.75 MPa) which indicates that 1 layer of CFRP with 9.525 mm radius will not result in crack re-initiation. Since the site conditions in the problem permit up to 10 mm crack stop hole radius, the assumed 1 layer of CFRP reinforcement with 9.525 mm crack stop hole radius is valid.

8. The steps from 3 to 7 are repeated for the case of 5 layers of CFRP. Five layers of CFRP is used in this example to demonstrate that higher factor of safety can be achieved for the problem under consideration. The corresponding RF value comes out to be 0.3858.

9.  $KI / \rho\alpha$  value corresponding to specimen reinforced with 5 CFRP layers will be 222.6 MPa ( $0.3858 \cdot 577$ ).

A nonlinear FEA carried out for the above conditions ( $2a = 44.45$  mm,  $\rho = 9.525$  mm,  $SR = 0, 0.08, 0.4$  and load = 51.7 MPa). The values calculated for  $KI / \rho\alpha$  of bare steel specimen and patched specimen with 1, 5 layers are 577.66 MPa, 296.2

MPa and 231.09 MPa, respectively. The corresponding RF values are 1, 0.51 and 0.4 respectively. It can be observed that the difference is 0.71% and 3.5% between proposed equation and FEA for a SR of 0.08 and 0.4 respectively, indicating the accuracy of the proposed equation.



## 2.6 References

Chung, K. (2003). "Mixed mode fatigue crack growth in aluminum plates with composite patches". *International Journal of Fatigue*, 25(4), 325-333.

Cory Arendt and C.T. Sun (1994). "Bending effects of unsymmetric adhesively bonded composite repairs on cracked aluminium panels". School of Aeronautics and Astronautics, West Lafayette, IN 47907

Hosseini-Toudeshky, H. (2006). "Effects of composite patches on fatigue crack propagation of single-side repaired aluminum panels". *Composite Structures*, 76(3), 243-251.

Hosseini-Toudeshky, H., Mohammadi, B., and Daghyani, H. (2006). "Mixed-mode fracture analysis of aluminium repaired panels using composite patches". *Composites Science and Technology*, 66(2), 188-198.

Kashfuddoja, M. and Ramji, M. (2014). "Critical analysis of adhesive layer behavior in patch-repaired carbon fiber-reinforced polymer panel involving digital image correlation". *Journal of Composite Materials*, 49(16), 2015-2028.

Khedkar, S., Chinthapenta, V., Madhavan, M., and Ramji, M. (2014). "Progressive failure analysis of CFRP laminate with interacting holes under compressive loading". *Journal of Composite Materials*, 49(26), 3263-3283.

Liu, H., Al-Mahaidi, R., and Zhao, X. (2009). "Experimental study of fatigue crack growth behaviour in adhesively reinforced steel structures". *Composite Structures*, 90(1), 12-20.

Liu, H., Zhao, X., and Al-Mahaidi, R. (2009). "Boundary element analysis of CFRP reinforced steel plates". *Composite Structures*, 91(1), 74-83.

Naboulsi, S. and Mall, S. (1996). "Modeling of a cracked metallic structure with bonded composite patch using the three layer technique". *Composite Structures*, 35(3), 295-308.

Reddy, S., Jaswanthsai, V., Madhavan, M., and Kumar, V. (2016). "Notch stress intensity factor for center cracked plates with crack stop hole strengthened using CFRP: A numerical study". *Thin-Walled Structures*, 98, 252-262.

Seo, D. and Lee, J. (2002). "Fatigue crack growth behavior of cracked aluminum plate repaired with composite patch". *Composite Structures*, 57(1-4), 323-330.

Shaat A, Schnerch D, Fam A, Rizkalla S. Retrofit of steel structures using fibre reinforced polymer (FRP): state-of-the-art. In: Transportation research board (TRB) annual meeting, Washington, DC; 2004

Shankar, K. and Wu, W. (2002). "Effect of welding and weld repair on crack propagation behaviour in aluminium alloy 5083 plates". *Materials & Design*, 23(2), 201-208.

Srilakshmi, R., Ramji, M., and Chinthapenta, V. (2015). "Fatigue crack growth study of CFRP patch repaired Al 2014-T6 panel having an inclined center crack using FEA and DIC". *Engineering Fracture Mechanics*, 134, 182-201.

Tsai, G. and Shen, S. (2004). "Fatigue analysis of cracked thick aluminum plate bonded with composite patches". *Composite Structures*, 64(1), 79-90.

Umamaheswar, T. and Singh, R. (1999). "Modelling of a patch repair to a thin cracked sheet". *Engineering Fracture Mechanics*, 62(2-3), 267-289.

## 2.7 Figure captions

Figure 1(a) and 1(b): Meshing around the crack stop hole

Figure 2: Areas of 0 degree ( $\text{mm}^2$ ), 25%, 50% and 75% stressed areas subjected to 103.4 MPa load

Figure 3: Areas of 15 degree ( $\text{mm}^2$ ), 25%, 50% and 75% stressed areas subjected to 103.4 MPa load

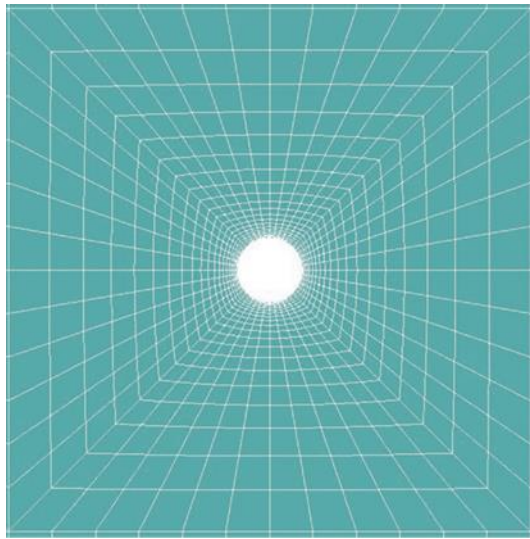
Figure 4: Areas of 45 degree ( $\text{mm}^2$ ), 25%, 50% and 75% stressed areas subjected to 103.4 MPa load

Figure 5: Areas of 60 degree ( $\text{mm}^2$ ), 25%, 50% and 75% stressed areas subjected to 103.4 MPa load

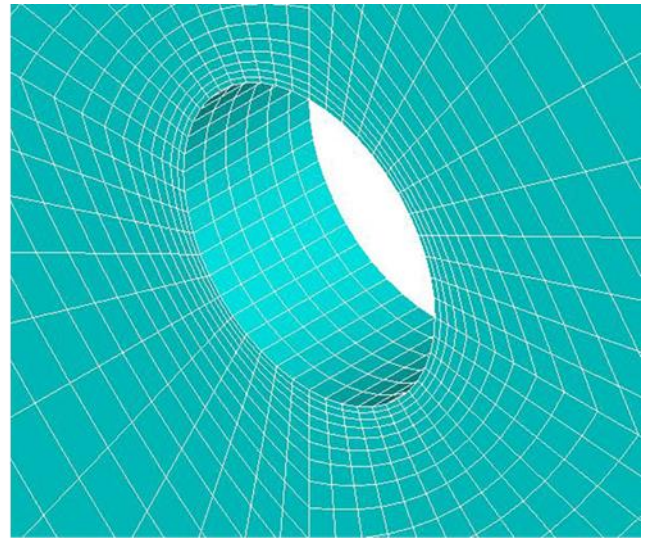
Figure 6: Variation of  $p_0$  to  $p_8$  with coefficients a, b, c, d and e

Figure 7:  $K_I / \rho^\alpha$  versus crack stop hole radius of bare steel specimen for 34.4 MPa load

Figure 8:  $K_I / \rho^\alpha$  versus crack stop hole radius of bare steel specimen for 51.7MPa load

















(a)













(b)







**Figure 1(a) and 1(b): Meshing around the crack stop hole**

| No. of layers | 25 % Yielded areas  | 50 % Yielded areas  | 75 % Yielded areas |
|---------------|---|---|--------------------|
| 9 layer       | <br>166.37 | 3.77<br> |                    |
| 8 layer       | <br>142.13 | 3.58<br> |                    |



|            |         |   |        |  |       |
|------------|---------|---|--------|--|-------|
| 7 layer    | 114.92  |    | 3.41   |     |       |
| 6 layer    | 108.58  |    | 2.47   |     |       |
| 5 layer    | 99.28   |    | 2.28   |     | 0.64  |
| 4 layer    | 91.06   |  | 2.53   |   | 0.64  |
| Bare steel | 7563.42 |  | 548.21 |  | 77.58 |

**Figure 2: Areas of 0 degree (mm<sup>2</sup>), 25%, 50% and 75% stressed areas subjected to 103.4 MPa load**












| No. of layers | 25 % Yielded areas  | 50 % Yielded areas   | 75 % Yielded areas |
|---------------|---|--|--------------------|
| 9 layer       | 162.72<br>   | 3.5<br>    |                    |
| 8 layer       | 141.54<br>  | 3.43<br>   |                    |
| 7 layer       | 122.79<br> | 3.01<br> |                    |
| 6 layer       | 100.69<br> | 2.88<br> |                    |
| 5 layer       | 93.79<br>  | 2.59<br> |                    |




|            |   |  |  |
|------------|---|--|--|
| 4 layer    | <br>83.37    | <br>2.25    | <br>0.69  |
| Bare steel | <br>7725.69 | <br>530.71 | <br>67.28 |

**Figure 3: Areas of 15 degree (mm<sup>2</sup>), 25%, 50% and 75% stressed areas subjected to 103.4 MPa load**

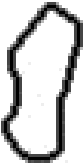

| No. of layers | 25 % Yielded areas   | 50 % Yielded areas   | 75 % Yielded areas |
|---------------|--|--|--------------------|
| 9 layer       | <br>61.21 | <br>2.05 |                    |













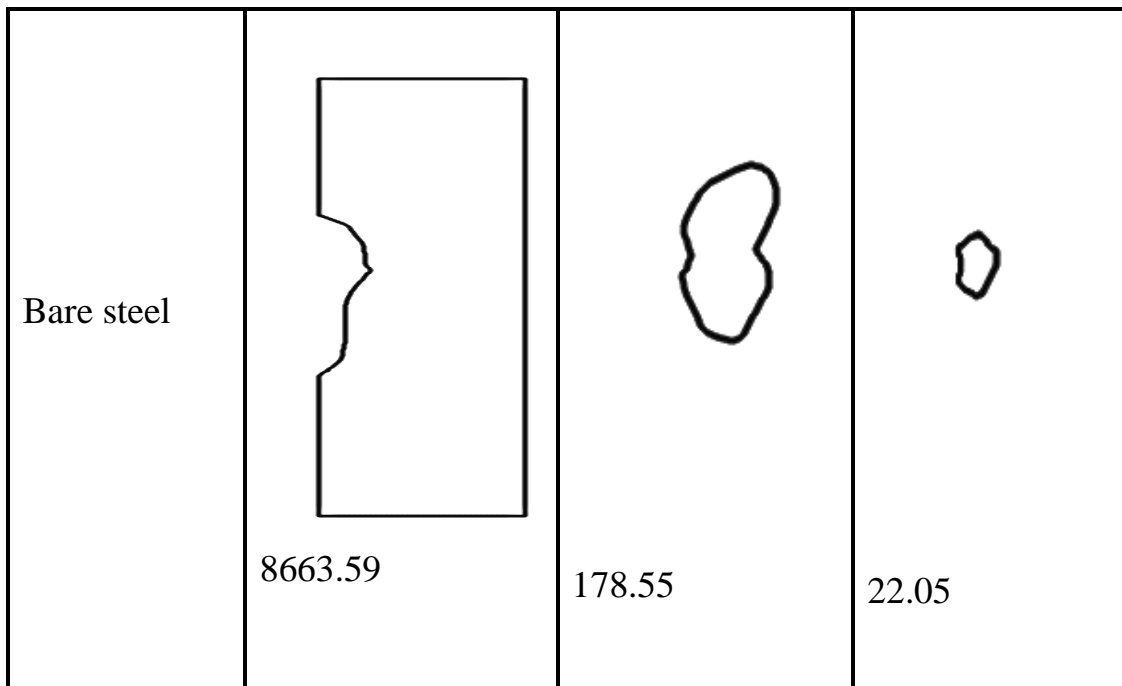
|         |        |   |      |  |   |
|---------|--------|---|------|--|---|
| 8 layer | 51.02  |    | 2.05 |   |   |
| 7 layer | 47.71  |    | 2.05 |   |   |
| 6 layer | 49.10  |    | 1.92 |    |   |
| 5 layer | 57.368 |  | 3.0  |  |   |
| 4 layer | 95.67  |  | 4.59 |  |  |
|         |        |   |      |  | 0.68  |

|            |   |   |   |
|------------|---|---|---|
| Bare steel |  |  |  |
|            | 7950.59   | 298.78  | 40.26   |

**Figure 4: Areas of 45 degree (mm<sup>2</sup>), 25%, 50% and 75% stressed areas subjected to 103.4 MPa load**

| No. of layers | 25 % Yielded areas   | 50 % Yielded areas | 75 % Yielded areas |
|---------------|--|--------------------|--------------------|
| 9 layer       | <br>65.26 |                    |                    |
| 8 layer       | <br>48.36 |                    |                    |

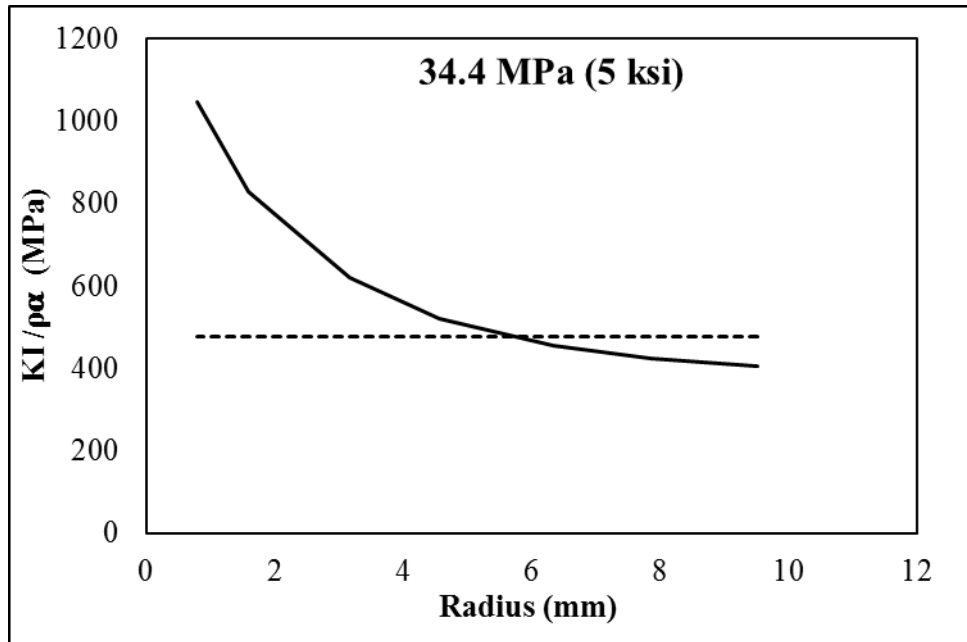
|         |        |   |      |   |   |
|---------|--------|---|------|---|---|
| 7 layer | 42.6   |    | 3.08 |    |   |
| 6 layer | 56.98  |    | 2.45 |   |   |
| 5 layer | 73.54  |   | 2.97 |    |    |
| 4 layer | 206.25 |  | 5.97 |  |  |



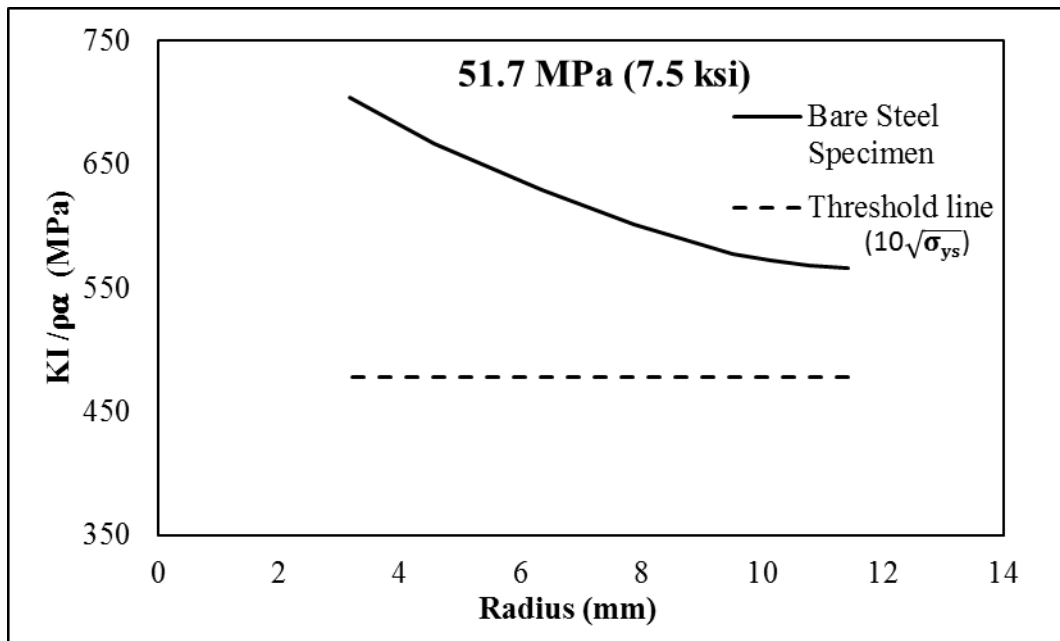
**Figure 5: Areas of 60 degree (mm<sup>2</sup>), 25%, 50% and 75% stressed areas subjected to 103.4 MPa load**

| Coefficients | Coefficients |        |        |        |      |
|--------------|--------------|--------|--------|--------|------|
|              | a            | b      | c      | d      | E    |
| <b>p0</b>    | -111         | 296    | -288   | 123    | -22  |
| <b>p1</b>    | 866          | -2280  | 2174   | -894   | 139  |
| <b>p2</b>    | 143          | -380   | 366    | -154   | 25   |
| <b>p3</b>    | -1798        | 4699   | -4425  | 1782   | -266 |
| <b>p4</b>    | 783          | -2105  | 2064   | -882   | 144  |
| <b>p5</b>    | -3005        | 7978   | -7702  | 3237   | -525 |
| <b>p6</b>    | 11390        | -29943 | 28460  | -11648 | 1794 |
| <b>p7</b>    | -5886        | 15336  | -14368 | 5729   | -836 |
| <b>p8</b>    | 898          | -2241  | 1969   | -707   | 85   |

**Figure 6: Variation of p0 to p8 with coefficients a, b, c, d and e**



**Figure 7:  $K_I/\rho^\alpha$  versus crack stop hole radius of bare steel specimen for 34.4 MPa load**



**Figure 8:  $K_I/\rho^\alpha$  versus crack stop hole radius of bare steel specimen for 51.7MPa load**

# Chapter 3

## Experimental study to halt the crack propagation by combined action of crack stop hole and CFRP laminates

### 3.1 Introduction

Various retrofitting techniques are employed to arrest the crack propagation which are originated due to fatigue loads in structural members. Any retrofitting method objective is to reduce the stress intensity factor (SIF). These retro fitting techniques are broadly classified into two groups (Shield et al. 2004): (a) Local retrofitting techniques: Crack stop holes, Peening, Gas Tungsten Arc (GTA) welding and (b) Global retrofitting techniques: use of Composite laminates. Generally, stress intensity factor is the term is used to measure the effect of crack. Depending on the relation between the load application directions, crack front and crack propagation there are three different types of stress intensity factors  $K_I$ ,  $K_{II}$  and  $K_{III}$ . If a crack stop hole is introduced at the end of a crack tip, the sharp crack gets blunted their by changing the stress intensity measurement from CSIF to NSIF. So, the present study is focused on the effect of combined action of crack stop hole and CFRP patches on cracked steel specimen.

### 3.2 Background

Tavakkolizadeh and Saadatmanesh (2003) and Jones (2003) worked on the strengthening the steel girders with CFRP patches against fatigue loading. Concluded that the fatigue life increases by 2 to 4 times than the unretrofitted specimens. Crack growth also decreases after attaching CFRP layers. Nozaka et al.

(2005) experimentally worked on the effective bond length of CFRP strips which are to fatigue steel bridge girders. Several types of adhesives, precured CFRP laminates and bonding configurations are studied to get the minimum bond length to achieve maximum strength of the repair technique. Proposed an analytical method to get shear strain distribution in the adhesive layer for estimating the effective bond length. Lenwari et al. (2006) worked experimentally and analytically on debonding strength of CFRP plates which are adhesively bonded. The effects of plate thickness, plate modulus, bondline thickness adhesive modulus and adhesive spew-fillet angle on stress intensity factor are discussed. Betti's law-based reciprocal work contour integral method (RWCIM) is used to calculate stress intensity factor. Observed the adhesive failure and concluded that the stress intensity factor is not sufficient to predict the debonding strength of the spew-fillet angle.

Kaan et al (2008) carried out experiments for fatigue enhancement of welded cover plates using CFRP composites. Developed a CFRP overlay doubler element with sufficient thickness to have a significant stiffening effect on the steel specimen. Results showed that, by attaching CFRP doubler elements reduces the stress demand at fatigue-critical welded connections. Concluded that the repair by CFRP overlays is the viable technique to increase the fatigue life of the bridge structures. Crain et al. (2010) studied analytically on development of a technique to improve fatigue lives of crack-stop holes in steel bridges. Used piezoelectric actuators operated at ultrasonic frequencies to convert electrical signals into mechanical work which produces residual compressive stresses that will expand crack stop holes. Investigated the potential of a technique to improve the fatigue life of undersized, crack-stop holes. Results of this study concluded that the fatigue capacity can be

increased when expansion on the order of 4% or more is achieved in crack-stop holes.

Alemdar et al. (2011a) and (2011b) experimentally worked to improve the bond between CFRP overlays and Steel for fatigue repairs. Embedded the breather fabric with in the layer of epoxy resin and studied the effect on bond strength and its performance under fatigue loading. Observed that the breather cloth eliminated large voids in the resin layer which decreases the initiation of fatigue cracks, increases peel strength and increases the residual capacity under monotonic loading. Under fatigue loading, retards the fatigue growth and increases the bond strength. Also studied parameters affecting the behaviour of CFRP overlay elements for fatigue vulnerable steel bridge girders. Studied experimentally and analytically the affect of configuration of a layer of resin, profile geometry of the composite overlay, and length of the composite overlay. Observed that the resin layer thickness has more effect on fatigue life than the geometric configuration of CFRP overlay. Analyses results showed that increase in resin layer thickness decreases the effectiveness in reducing the stress demand at critical locations and decreases the shear demand at the interface between resin layer and steel.

Hmidan et al. (2011) experimentally studied the behaviour of notched beams repaired with CFRP sheets with various initial crack configurations subjected to flexural load. Various notch sizes are created by varying notch depth and beam height ratio. Observed that the initial damage affects the plastic region near the notch tip, rate of web fracture and initiates the debonding of CFRP. Concluded that the fracture energy and the crack tip plasticity are improved by the CFRP repair.



Alemdar et al. (2012) carried out experimental tests and analytical simulations to investigate the fatigue performance coverplate specimens in which the welded connections were reinforced with CFRP overlays. Observed that, by introducing breather cloth within the bond layer, the fatigue strength of the bond layer was drastically improved. Results showed that, Using CFRP overlays reduces the stress demand which will increase the fatigue life of the welded connection and CFRP overlays reduces the stress range at the critical point. Finally concluded that the CFRP repair technique is more effective under field conditions.

Kaan et al. (2012) experimentally worked on the fatigue enhancement of welded connections using CFRP sheets. Seven specimens are tested in which four are CFRP strengthened and three are controlled specimens. Strengthened specimens shown has shown the increased stiffness, reduced stress demand at fatigue-vulnerable welds, increased the fatigue life and improved fatigue performance of connections. Observed that the composition and thickness of the resin layer are important for bond strength and identified an optimal bond composition for excellent fatigue performance. Wang et al. (2014) experimentally and analytically analysed the parameters influencing the fatigue repair effectiveness by varying FRP configurations. Three different types of configurations and their effect on crack growth life are studied. Among them the configuration which has more FRP thickness, thinner adhesive thickness and shorter crack length is more effective than other configurations. Ghahremani et al. (2015) and Ghahremani (2014) worked experimentally and analytically on inhibiting the distortion created by fatigue in steel girders using FRP angles. Adhesively bonded FRP angles are attached to the web stiffeners ends in steel bridge girders subjected to fatigue loading. Observed

that after repairing with FRP angles fatigue life is increased by hundred percent. Concluded that the FRP based retrofit method is more efficient than other conventional repair methods.

Qian Yu et al. (2015) investigated the fatigue crack propagation for CFRP strengthened steel plates with longitudinal weld attachments by using boundary element analysis. Investigated on the effects of double sided strengthening, double sided weld attachment and CFRP stiffness on the fatigue behaviour of welded joints. Concluded that double sided repair is more efficient than the single sided repair. Xie et al. (2015) experimentally worked on crack detecting methods and their repair technology based on fatigue crack features in steel box girders. Results shown that, by using ultrasonic techniques length, depth, angle and location of the crack can be detected. Concluded that the inclined hole is better than the normal vertical stop hole in reducing the stress concentration and for better stress distribution. Abbas and Eatherton (2015) experimentally worked on total of 48 cyclic bend tests and monotonic axial tests to study the effect of defect repair and deck attachment on low cycle fatigue resistance of steel moment frame beams. Six type of specimens including bare specimens, and several types of fasteners and repairs methods are used. Elongation at fracture is reduced for monotonic tests and under cyclic tests the number of cycles to initiate fracture and number of cycles to full fracture of specimen are reduced after repairing. Simmons et al. conducted experiments to improve fatigue performance of drilled holes in steel bridges by use of mechanical treatments. A total of 15 fatigue specimens, examining levels of retained expansion in 16 specimens and mechanical treatments studied were cold-expansion of drilled holes and a newly-developed technique termed Piezoelectric Impact Compressive

Kinetics (PICK) treatment. Both techniques are capable of producing enough permanent retained expansion (RE) to improve fatigue life, but PICK-treatment of drilled holes shows greater fatigue lives and higher retained expansion (RE) values than cold-expansion treatment.

### **3.3 Experimental study**

#### **3.3.1 Materials and Specimen**

The experimental studies were performed at the Structures Laboratory of Indian Institute of Technology. To study the combined action of crack stop hole and CFRP laminates,

total of 15 steel specimens were tested in which 5 are single side repaired and 5 are double side repaired specimens with CFRP laminates and another 5 specimens are non-strengthened specimens with crack stop hole.

#### **3.3.2 Material properties**

The steel plates were 4 mm thick with nominal yield strength of 470 MPa and the nominal ultimate tensile strength is 570 MPa. The mechanical properties of the steel plates were measured using tensile coupon tests according to ASTM standards and the results are listed in table 1. Stress strain curve of the steel plate is provided in Fig. 1.

Uniaxial CFRP laminates of thickness 0.3mm is provided as a layer of dimensions 200mm long 160mm wide on the steel plate. The material properties of CFRP plates were obtained by coupon tests according to ASTM standards which are given in

table 2. The stress strain curve of the CFRP is provided in Fig. 2. Epoxy resin was used as bonding adhesive, and its properties are also given in table 2.

### **3.3.3 Coupon test for material properties**

A total of 3 steel coupons and 3 CFRP coupons are tested to calculate the material properties of the steel specimen and CFRP laminates respectively. Each coupon has a gauge length of 150mm and steel coupon has a width of 12.5mm and thickness of 4mm. After testing, the Elastic modulus of steel is  $2.1E5\text{Mpa}$  and CFRP has an Elastic modulus of  $122.48E3\text{Mpa}$ . Fig. 3 (a) and 3 (b) shows the coupons of steel and CFRP respectively after testing.

### **3.3.4 Specimen Preparation**

The specimens were repaired by combined action of crack stop hole and CFRP laminates bonded on single side and double side of cracked steel plates by epoxy adhesive, as shown in Fig. 4. The dimensions of the geometry of the steel specimens are 600mm long, 160mm wide and 4mm thick. All steel plates were machined with a centre crack of 25 mm length made by wire cutting in EDM (Electrical discharge machining) and the crack stop holes were drilled at the ends of the crack by drilling machine as shown in Fig. 5 (a) and Fig. 5 (b). Various parameters considered in the study are listed in table 3.

The surfaces of the steel specimens were cleaned using a sand paper to create smoothness, and to ensure the effective bond between the CFRP and steel specimen. The surfaces were then cleaned with acetone before the adhesive application to remove grease and dust and to expose a fresh chemically-active surface to ensure

better mechanical interlocking. A thin layer of adhesive of 0.3 thickness was then applied uniformly using a brush. CFRP laminates were then attached onto the adhesively-coated steel plates. Finally, a concrete block was placed on top of the CFRP plates to apply uniform pressure until extra adhesive and air pockets were forced to bleed out. The specimens were cured for a week before the testing.

Prior to bonding with adhesive, the strain gauges are arranged along the crack stop hole at crack level to measure the characteristic distance  $X_c$  (distance from the hole edge up to which the stress remains constant) and stress gradient  $\alpha$  (linear decrease in stress). After attaching CFRP the strain gauges are attached to measure the  $X_c$  and  $\alpha$ . The total set up of strain gauges of bare steel specimen, single side repaired specimen and double side repaired are shown in the Fig. 6(a), 6(b) and 6(c) respectively.

### **3.3.5 Static tensile testing**

The tests are carried out on a pneumatic UTM machine of 150KN capacity. The testing set-up is shown in Fig. 7. This photograph was taken at the time of testing. A load of 100KN was applied on the steel plate, so that a stress of 156Mpa is on the steel specimen. At that particular loading, the readings were taken to study the combined action of crack stop hole and CFRP laminates.

### **3.4 Experimental results**

This experimental study is aimed at studying the combined action of crack stop hole and the CFRP patch in arriving at the appropriate crack stop hole radius when subjected to static tensile load. Prior to the combined effect, the effect of bare steel

specimen was studied to understand the effect of hole radius in crack retardation. The stress intensity factor was calculated using NSIF which includes the effect of  $X_c$  and  $\alpha$ . Henceforth, the experimental study was carried out for the combined action of crack stop hole and CFRP patch were based on NSIF.

### 3.4.1 NSIF calculation

The literature review indicates that the crack initiation life ( $N_i$ ) of a notch is typically expressed as a function of  $K_I / \sqrt{r}$ , which is based on LEFM. In LEFM frame work, the stress gradient is expressed as a function of  $1 / \sqrt{r}$ , singularity which indicates that when the radius approaches zero, it behaves like a sharp crack. However, the LEFM assumption is not valid if loading, crack geometry and the specimen thickness leads to yielding at notch tip. Hence NSIF is preferred than CSIF.

The output from experimental study is used to determine  $X_c$  and  $\alpha$  needed to evaluate NSIF using Eq. 1, which is given by Boukharouba et al. [19].

$$K_{\rho} = \sigma_{yy}(X_c) * \sqrt{2\pi} \left( X_c + \frac{\rho}{2} \right)^{\alpha}$$

where,  $\sigma_{yy}$ = Stress at characteristic distance  $X_c$ ,  $\rho$ = Radius of the notch and  $\alpha$ = Stress gradient. Fig. 7 shows a typical variation in stress ahead of a crack stop hole in a log-log plot for one particular case of bare steel specimen.

### **3.4.2 Characteristic distance ( $X_c$ ) calculation**

The distance from the hole edge up to which the stress remains constant is called as the characteristic distance in Fig. 7. In general, the  $X_c$  value ranges between 1mm to 2mm from crack stop hole edge. But in experimental study the width of each strain gauge is 4.5mm which became impossible to find the  $X_c$  value. Hence a linear curve is developed for different crack stop hole radii and the  $X_c$  values from the numerical analysis a shown in Fig. 19. From this plot the  $X_c$  values are absorbed for different crack stop hole radii.

### **3.4.3 Stress gradient ( $\alpha$ ) calculation**

The linear decrease in stress along the crack of the plate is called as stress gradient shown in Fig. 7. A total of 8 strain gauges are used on bare steel specimen to calculate the stress gradient. These strain gauges are attached near the crack stop hole at the crack level. The plot between for stress gradient was done by applying logarithmic function to the distance from crack stop hole values and stress values and they are plotted in a regular graph which implies the logarithmic plot. The value of stress gradient is calculated and compared with analytical values as shown in Fig. 16.

For single sided repair, a total of 24 strain gauges are used on each specimen. A total of 8 strain gauges are attached in between the CFRP and steel near the crack stop hole at the crack level and 8 more strain gauges are attached on the CFRP approximately near the crack stop hole at the crack level and remaining 8 are

attached on the another side (unpatched side) of specimen. The value of stress gradient is calculated and compared with analytical values as shown in Fig. 17.

For double sided repair also a total of 24 strain gauges are used on each specimen. A total of 8 strain gauges are attached in between the CFRP and steel near the crack stop hole at the crack level and 8 more strain gauges are attached on the CFRP approximately near the crack stop hole at the crack level and remaining 8 are attached on the another side (right side) of specimen for double sided repair. The value of stress gradient is calculated and compared with analytical values as shown in Fig. 18.

The various configurations of strain gauges are shown in the Fig. 6 (a), 6 (b) and 6 (c).

#### **3.4.4 Optimum crack stop hole radius calculation**

Calculate  $K_I / \rho^\alpha$  of a bare steel specimen and plot the variation of the same with respect to various crack stop hole radii as shown in Fig. 9. Plot the threshold line given by Barsom [8] (Eq. 2) in the same plot of  $K_I / \rho^\alpha$  versus crack stop hole radii to determine the threshold radius.

$$\frac{K_I}{\sqrt{\rho}} = 10\sqrt{\sigma_{ys}} \quad (2)$$

In the figure, there is no intersection between the threshold line and the bare steel specimen curve obtained from experimental study indicating that a CFRP patch is mandatory (crack stop hole alone is not enough) to reduce the SIF.

#### **3.4.5 Stress intensity factor vs crack stop hole radii**



After calculating the  $K_I / \rho^\alpha$  from eq. 1, the results were expressed and compared analytically by finite element analysis in the form of graphs in Fig. 10. The results shows that, as crack stop hole size increases the  $K_I / \rho^\alpha$  decreases for all specimens including bare steel specimen.

In Fig. 11 compares the efficiency of various repair techniques. This shows that the single sided repair is better than using the crack stop hole alone and the double sided repair is far better than the two techniques mentioned above to reduce the stress intensity factor and finally for arresting the crack propagation.

### **3.4.6 Reduction Factor (RF)**

To account for the effect of CFRP patch in stress reduction, a reduction factor (RF) is introduced.

$$\text{Reduction factor} = \frac{(K_I / \rho^\alpha) \text{with CFRP}}{(K_I / \rho^\alpha) \text{without CFRP}} \quad (2)$$

The reduction factor for different radii at a load of 156.25Mpa for both single sided repair and double sided repair is compared and shown in the Fig. 12. The results shows that the double sided repair is more efficient than the single sided repair.

## **3.5 Verification of experimental results by using FEA**

### **3.5.1 Geometry and finite element model**

The specimen geometry is same as in the experimental study mentioned above. The dimensions of the specimen are given in Table 1 and its geometry is shown in the fig 13.

A magnitude of 156.25Mpa load is applied. The connection between CFRP, steel plate and CFRP, adhesive, shown in Fig. 14 are modeled using bonded contact. In bonded contact, contacting surfaces are assumed to be glued together throughout the analysis. To create bonded contact, contact and target elements needs to be defined on the faces of elements, where they come into contact. In this study multi point constraint (MPC) algorithm is used for bonded contact.. The CFRP material properties are taken from the experimental study mentioned above and in the present study, the one layer of CFRP is used in the analysis. The thickness of the lamina reported as 0.3mm and CFRP patch length (l) is taken as 200 mm based on the experimental study. The properties of composite lamina and adhesive are given in the Table 2.

Incremental meshing as given in [22] is employed around the hole (Fig. 15) to capture the sharp stress gradient because the value of stress at the edge of the hole is sensitive to element size. The number of elements used around the hole is 6 elements in thickness direction, 20 elements in radial direction and 48 elements in angular direction. Although the applied loads are less than the yield stress of steel, localized yielding occurs at crack tip. Therefore, to take into account the local yielding behavior, a nonlinear Finite Element Analysis (FEA) is carried out in this research work using ANSYS 12.0 software. For modeling all components (i.e. steel plate, adhesive, and CFRP plate) Solid 186 element is used. Solid 186 element has mid side nodes and it performs better in stress singularity regions and for nonlinear analysis.

### **3.6 Results and discussion**

To validate the experimental study, the analysis was ran at the same load 156.25Mpa for the steel specimens mentioned above.

To calculate the stress intensity factor, characteristic distance and stress gradient are to be calculated. The characteristic distance ( $X_c$ ) is not going to change from experimental values because it was absorbed from the analysis itself. The stress gradient ( $\alpha$ ) is calculated from the results. In analysis at each and every point near the crack stop hole along the crack level was taken but in experimental studies only 8 strain gauges are placed to calculate stress gradient. So there exists a slight difference between the experimental gradient and analytical gradient.

Fig. 16, 17 and 18 shows the stress gradient lines for all the specimens for different crack stop hole radii. Fig. 10 shows the variation between experimental results and FEA results of  $K_I/\rho^\alpha$  vs crack stop hole radii. The difference in between the results is due to variation of stress gradient and stress values at  $X_c$  ( $\sigma_{yy}$ ) between experimental results and FEA results.

In general, the strain gauges are to be placed at the edge of the crack stop hole to calculate the  $\sigma_{yy}$ , but due to CFRP wrapping the strain gauges are impossible to place exactly at the edge of the hole. Due to the approximation of the strain gauge placements the difference between the experimental results and analytical results arises.

### **3.7 Conclusion**

This numerical study focuses on fracture mechanics approach to evaluate the effectiveness of the combined action of crack stop hole and CFRP patch. The study

is to determine the appropriate crack stop hole radius for bare steel specimen by using NSIF equation rather than CSIF due to the un-conservative nature. In the present study, crack stop hole serves as a notch and it is assumed that the crack originates from the edge of the hole. The application of CFRP will retard the crack re-initiation by reducing the stress value and there is no influence of inclination of crack, because the condition of plate with crack is changed to plate with hole.

The application of CFRP will retard the crack re-initiation by reducing the stress value. The effect of patch thickness on the reduction of stress is calculated in terms of stiffness ratio and it is observed that stress is reduced by 92% and 16% at a stiffness ratio of 0.96 and 0.16 respectively. The applicability of the developed reduction factor is demonstrated using a numerical example and validated by FEA.

The studies indicate that there is a significant reduction in  $KI / \rho^\alpha$  on patched side by using CFRP patch, the value of which reaches a minimum and then exhibits asymptotic behavior with increase in SR. This means that the effectiveness of a CFRP patch ceases to reduce the SIF when the additional thickness due to loading eccentricity results in excessive bending of the specimen.

The load that applied on the specimen is too low to effect the bond between the CFRP and steel, hence it should be recognized that the current formulation of perfect bonding between steel and CFRP layers may not reflect reality. However, the significant improvement in stress reduction after shows the potential of the proposed retrofit and the results shows that the double sided repair is better than the single sided repair.

### 3.8 References

- Alemdar, F., Gangel, R., Matamoros, A., Bennett, C., Barrett-Gonzalez, R., Rolfe, S., and Liu, H. (2014). "Use of CFRP Overlays to Repair Fatigue Damage in Steel Plates under Tension Loading". *J. Compos. Constr.*, 18(4), 04013052.
- Crain, J., Simmons, G., Bennett, C., Barrett-Gonzalez, R., Matamoros, A. and Rolfe, S. (2010) "Development of a technique to improve fatigue lives of crack-stop holes in steel bridges". *Transportation Research Record: Journal of the Transportation Research Board*
- Erdogan, F., and Sih, G. (1963). "On the Crack Extension in Plates Under Plane Loading and Transverse Shear". *Journal of Basic Engineering*, 85(4), 519.
- Ghahremani, K., Walbridge, S., and Topper, T. (2015). "Inhibiting Distortion-Induced Fatigue Damage in Steel Girders by Using FRP Angles". *J. Bridge Eng.*, 20(6), 04014085.
- Hmidan, A., Kim, Y., and Yazdani, S. (2011). "CFRP Repair of Steel Beams with Various Initial Crack Configurations". *J. Compos. Constr.*, 15(6), 952-962.
- Jones, S., and Civjan, S. (2003). "Application of Fiber Reinforced Polymer Overlays to Extend Steel Fatigue Life". *J. Compos. Constr.*, 7(4), 331-338.
- Kaan, B., Alemdar, F., Bennett, C., Matamoros, A., Barrett-Gonzalez, R., and Rolfe, S. (2012). "Fatigue Enhancement of Welded Details in Steel Bridges Using CFRP Overlay Elements". *J. Compos. Constr.*, 16(2), 138-149.
- Lenwari, A., Thepchatri, T., and Albrecht, P. (2006). "Debonding Strength of Steel Beams Strengthened with CFRP Plates". *J. Compos. Constr.*, 10(1), 69-78.
- Nozaka, K., Shield, C., and Hajjar, J. (2005). "Effective Bond Length of Carbon-Fiber-Reinforced Polymer Strips Bonded to Fatigued Steel Bridge I-Girders". *J. Bridge Eng.*, 10(2), 195-205.
- Tavakkolizadeh, M., and Saadatmanesh, H. (2001). "Galvanic Corrosion of Carbon and Steel in Aggressive Environments". *J. Compos. Constr.*, 5(3), 200-210.

- Tavakkolizadeh, M., and Saadatmanesh, H. (2003). "Fatigue Strength of Steel Girders Strengthened with Carbon Fiber Reinforced Polymer Patch". *Journal of Structural Engineering*, 129(2), 186-196.
- Wang, H., Wu, G., and Wu, Z. (2014). "Effect of FRP Configurations on the Fatigue Repair Effectiveness of Cracked Steel Plates". *J. Compos. Constr.*, 18(1), 04013023.
- Xie, F., Ji, B., YuanZhou, Z., Fu, Z., and Ge, H. (2015). "Ultrasonic Detecting Method and Repair Technology Based on Fatigue Crack Features in Steel Box Girder". *J. Perform. Constr. Facil.*, 04015006.
- Yu, Q., Chen, T., Gu, X., Zhao, X., and Xiao, Z. (2015). "Boundary Element Analysis of Fatigue Crack Growth for CFRP-Strengthened Steel Plates with Longitudinal Weld Attachments". *J. Compos. Constr.*, 19(2), 04014044.

### 3.9 Figure captions

- Figure 1: Stress strain curve of steel specimen
- Figure 2: Stress strain curve of CFRP
- Figure 3: Coupons after testing (a) steel coupons (b) CFRP coupons
- Figure 4: from AutoCAD
- Figure 5(a): Sample of crack stop hole and crack
- Figure 5(b): Samples of crack stop hole radii, crack and strain gauges arrangement
- Figure 6(a): Strain gauges configuration for bare steel specimen
- Figure 6(b): Strain gauges configuration for single side repaired specimen
- Figure 6(c): Strain gauges configuration for double side repaired specimen
- Figure 7: Test setup
- Figure 8: Stress distribution ahead of crack stop hole
- Figure 9: Calculation of optimum crack stop hole radii
- Figure 10(a):  $KI/\rho^a$  vs crack stop hole radii of bare steel specimen
- Figure 10(b):  $KI/\rho^a$  vs crack stop hole radii of single sided repair
- Figure 10(c):  $KI/\rho^a$  vs crack stop hole radii of double sided repair
- Figure 11:  $KI/\rho^a$  vs crack stop hole radii of various repair techniques
- Figure 12: RF vs crack stop hole radii for one layer of CFRP
- Figure 13: Geometry of the specimen in ANSYS
- Figure 14(a): Modelling of single sided specimen
- Figure 14(b): Modelling of double sided specimen
- Figure 15(a): Meshing around the crack stop hole in radial and angular direction
- Figure 15(b): Meshing around the hole in thickness direction
- Figure 16: Stress gradient for bare steel specimen for (a) 6.5mm radius, (b) 8.5mm radius, (c) 10mm radius, (d) 14mm radius and (e) 18mm radius
- Figure 17: Stress gradient for single side specimen for (a) 6.5mm radius, (b) 8.5mm radius, (c) 10mm radius, (d) 14mm radius and (e) 18mm radius

Figure 18: Stress gradient for double side specimen for (a) 6.5mm radius, (b) 8.5mm radius, (c) 10mm radius, (d) 14mm radius and (e) 18mm radius

Figure 19: Calculation of  $X_c$  at desired crack stop hole radiu



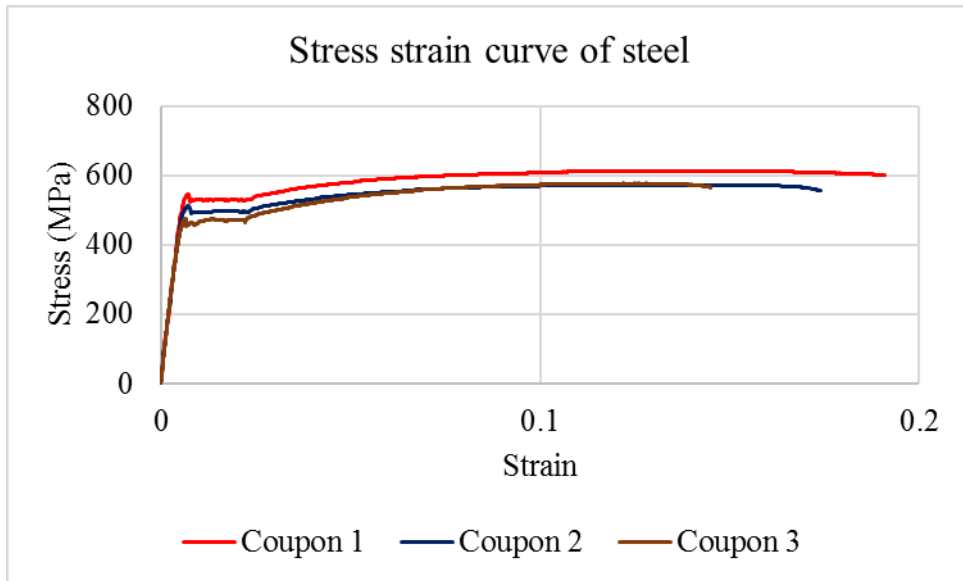


Figure 1: Stress strain curve of steel specimen

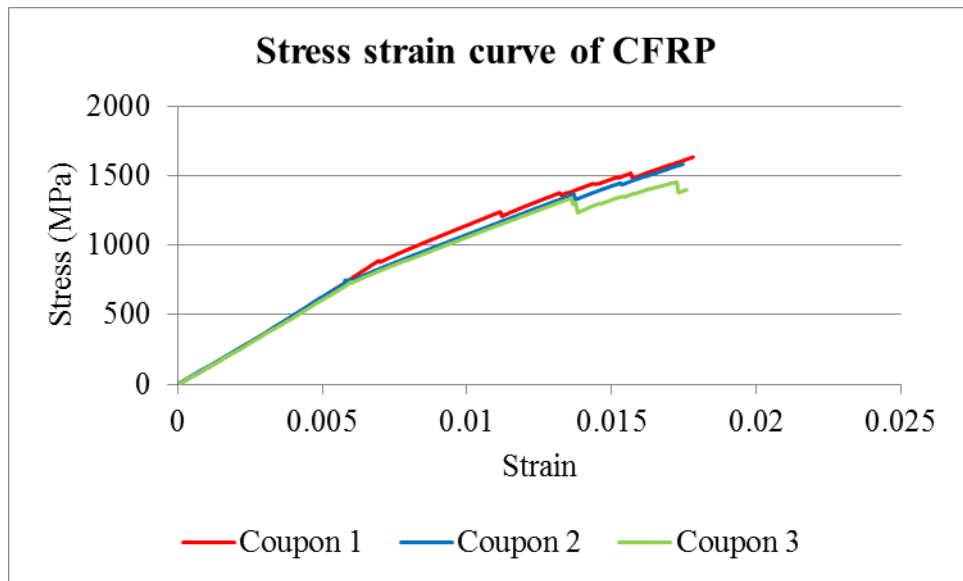
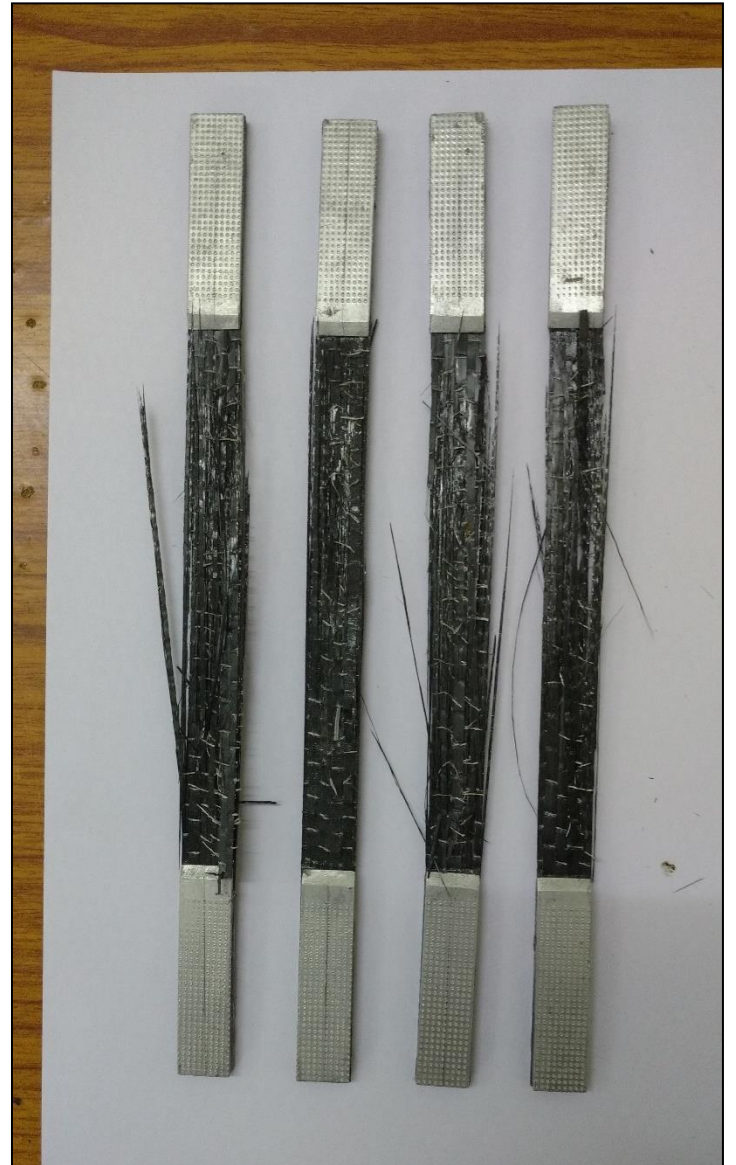


Figure 2: Stress strain curve of CFRP

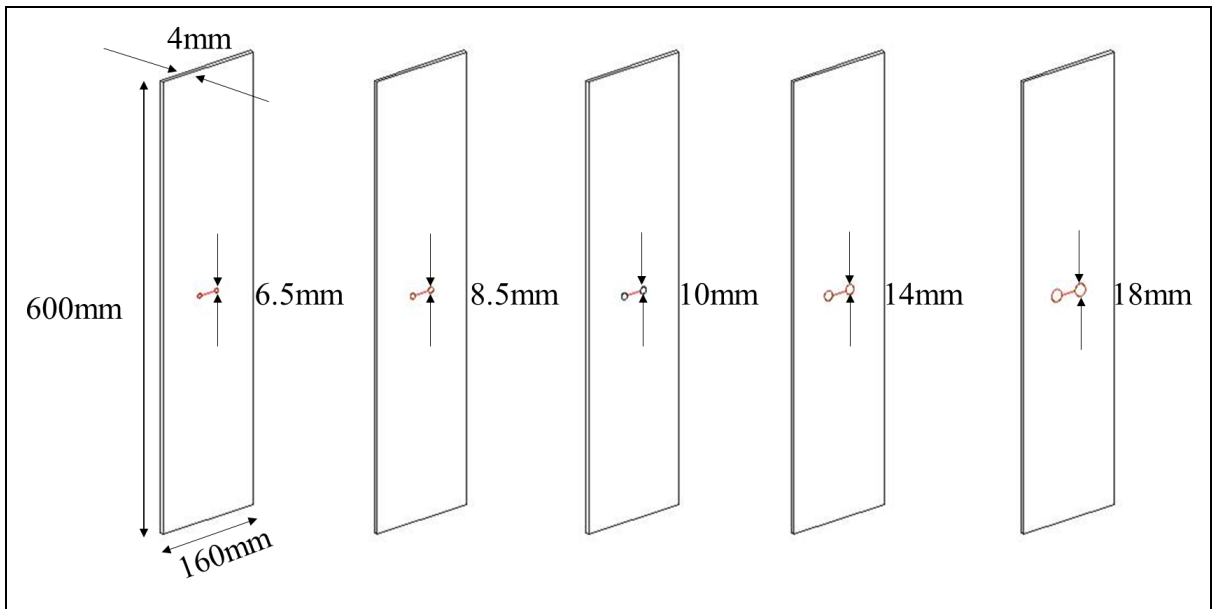


(a)

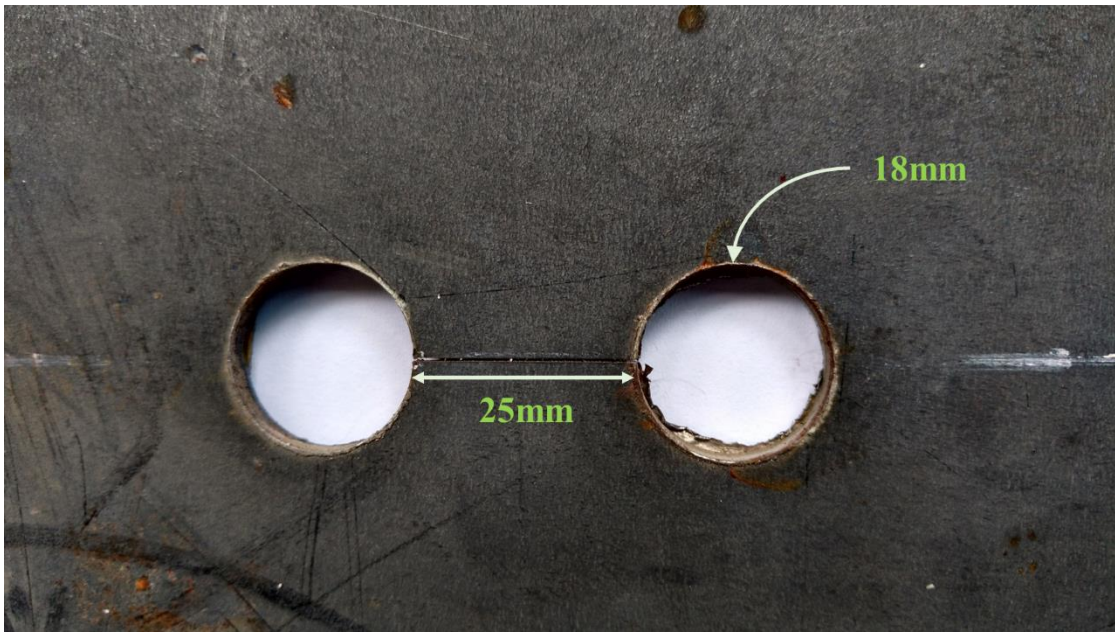


(b)

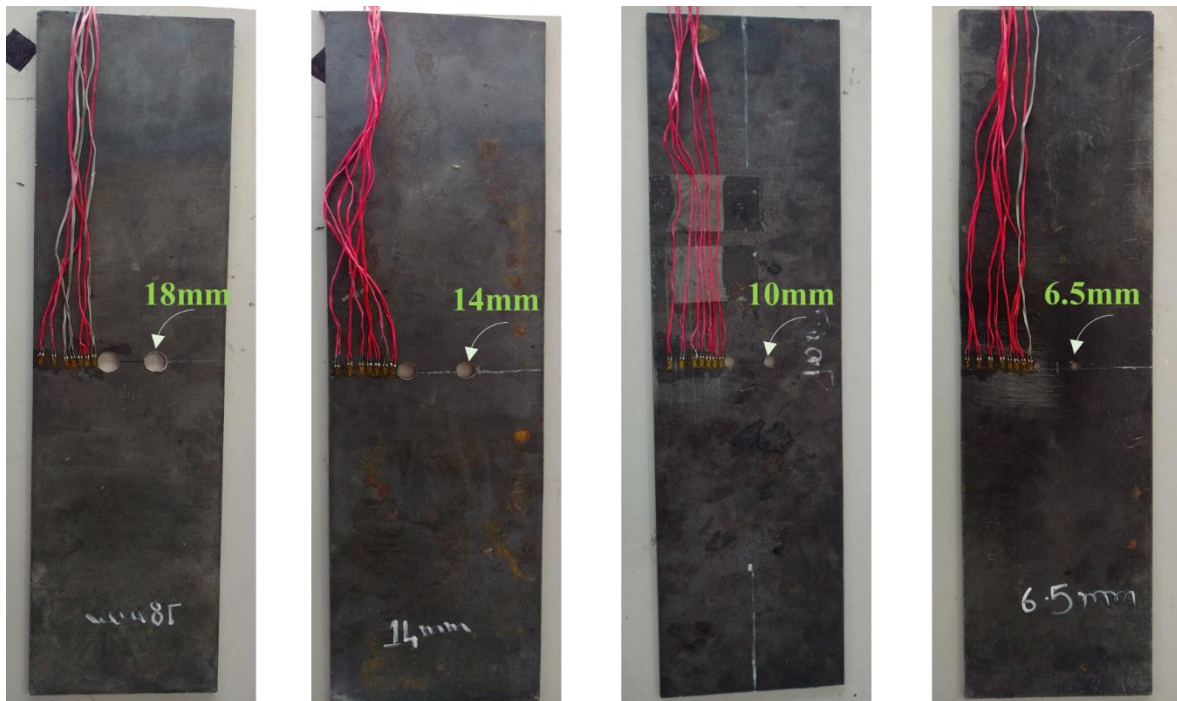
Figure 3: Coupons after testing (a) steel coupons (b) CFRP coupons



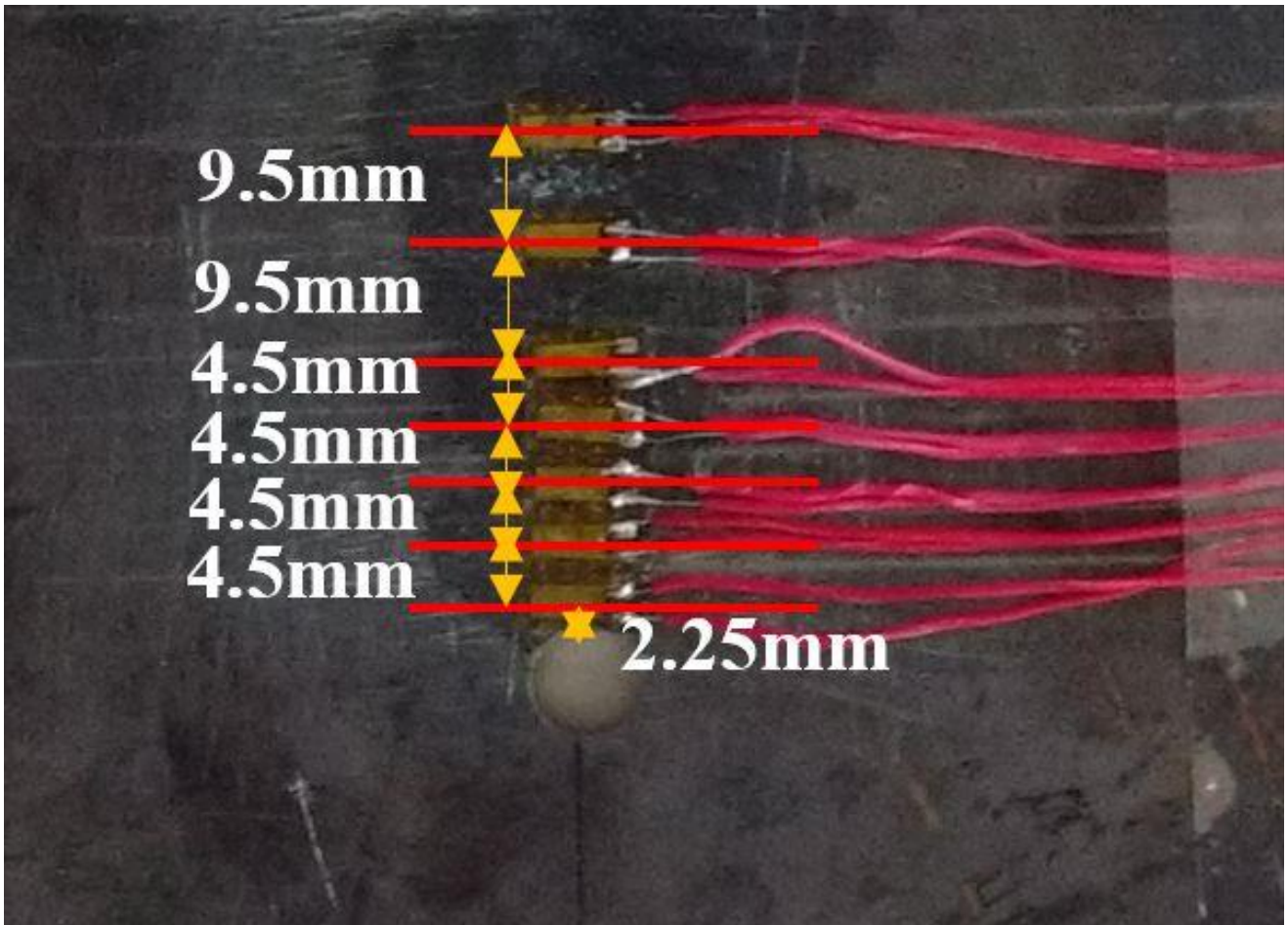
**Figure 4: Geometry of the specimen**



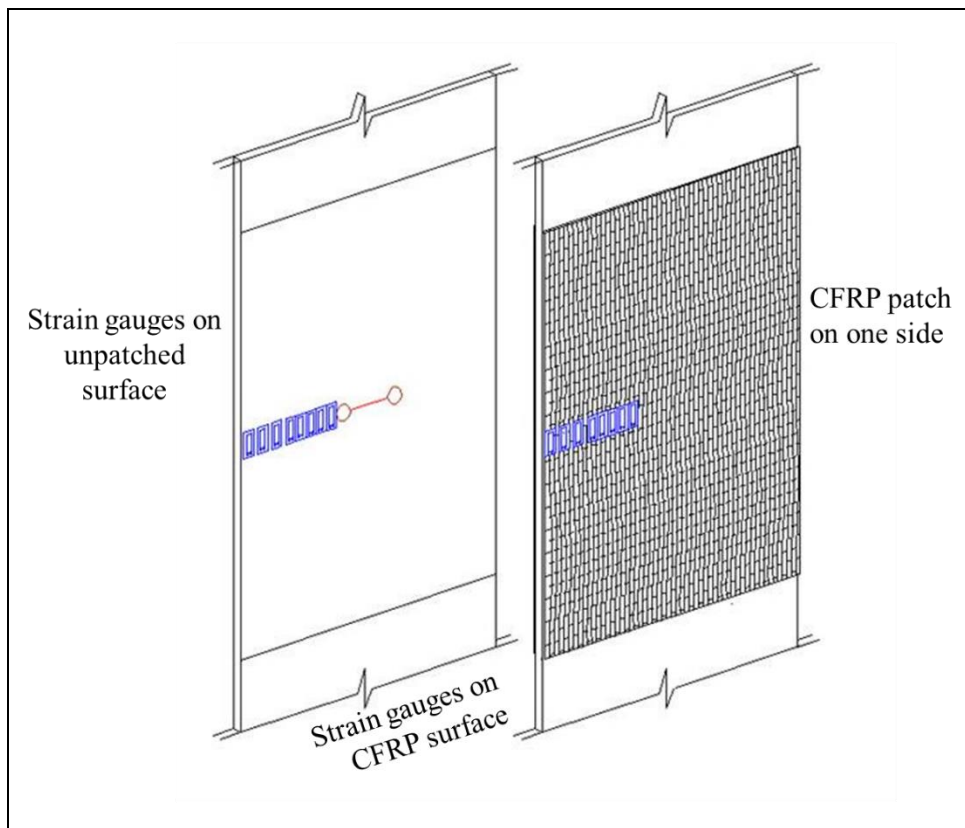
**Figure 5(a): Sample of crack stop hole and crack**



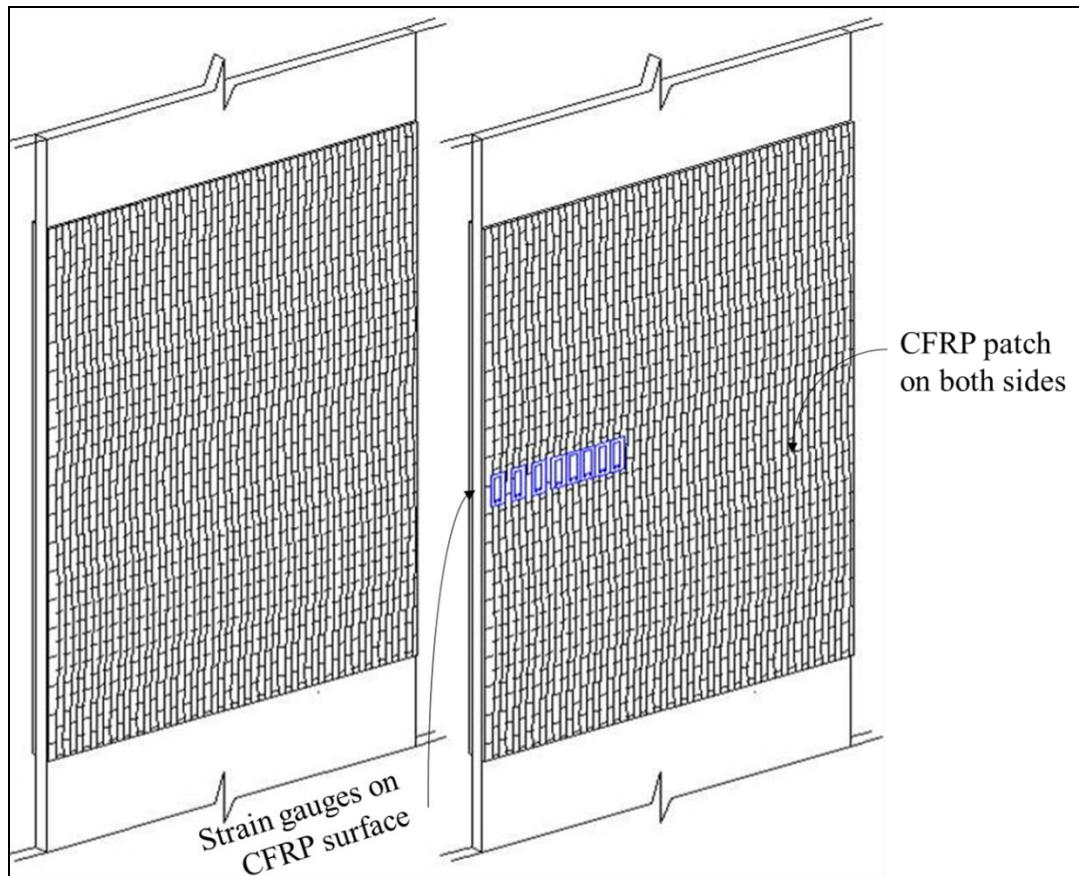
**Figure 5(b): Samples of crack stop hole radii, crack and strain gauges arrangement**



**Figure 6 (a): Strain gauges configuration for bare steel specimen**



**Figure 6 (b): Strain gauges configuration for single side repaired specimen**



**Figure 6 (c): Strain gauges configuration for double side repaired specimen**

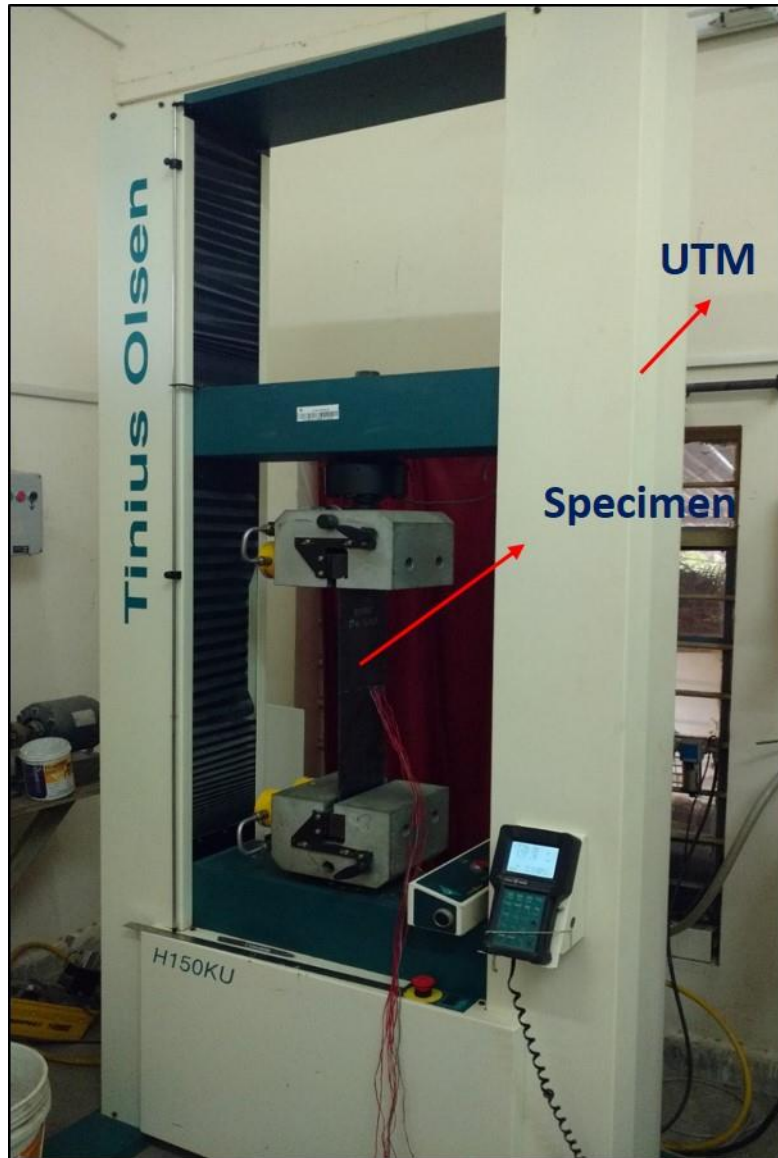


Figure 7: Test setup



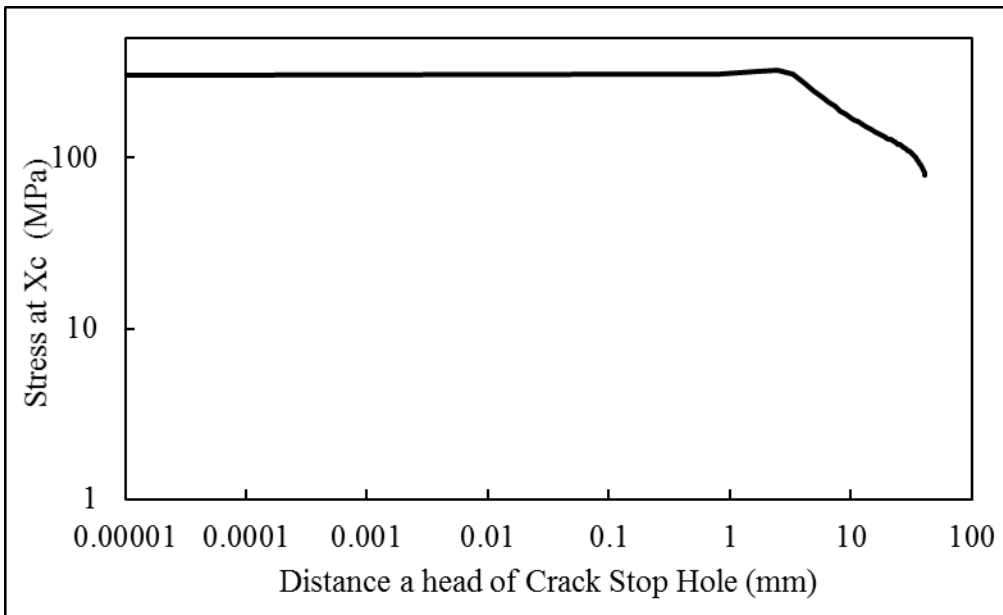


Figure 8: Stress distribution ahead of crack stop hole

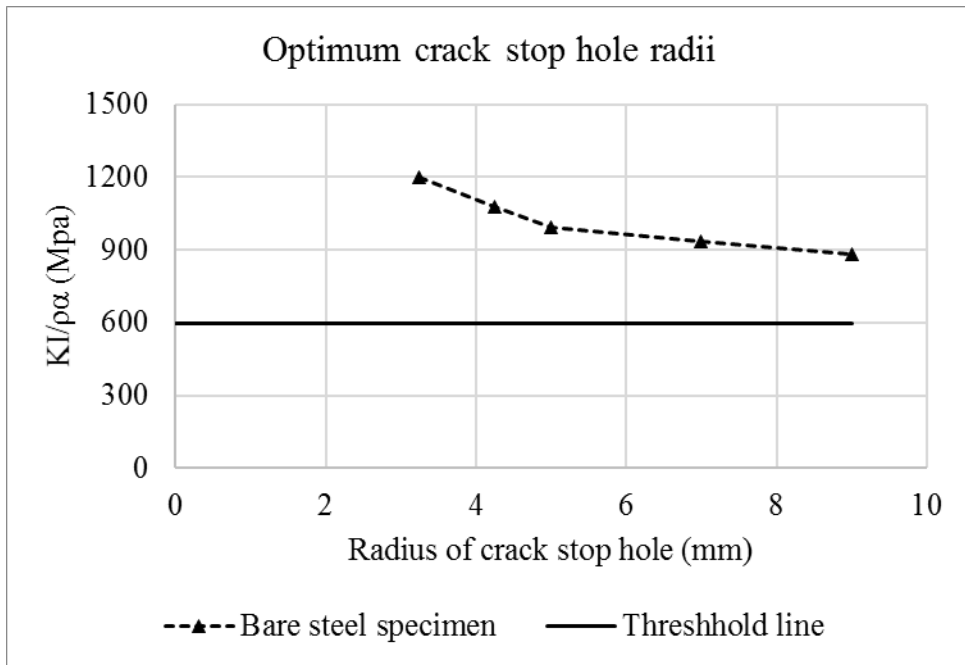


Figure 9: Calculation of optimum crack stop hole radii

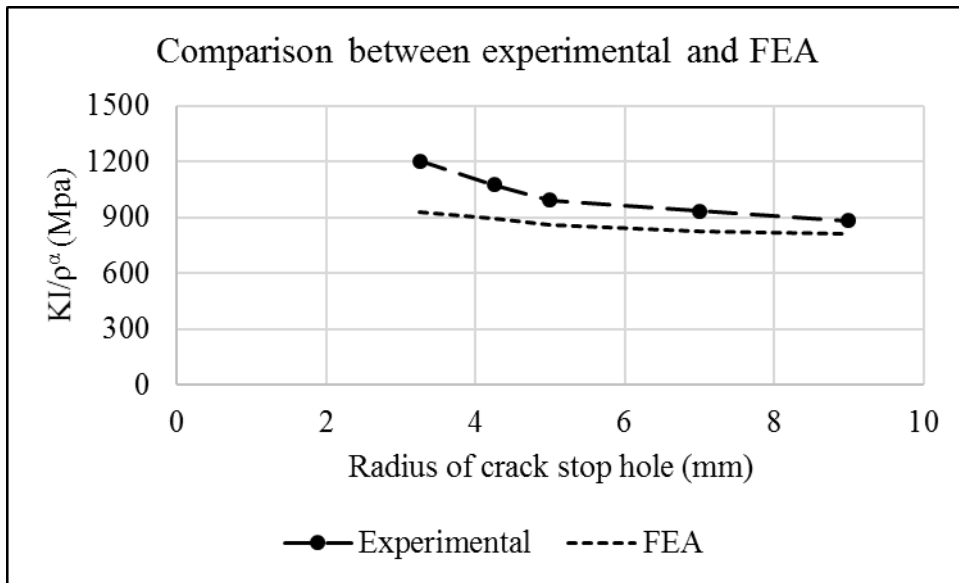


Figure 10 (a):  $KI/\rho^\alpha$  vs crack stop hole radii of bare steel specimen

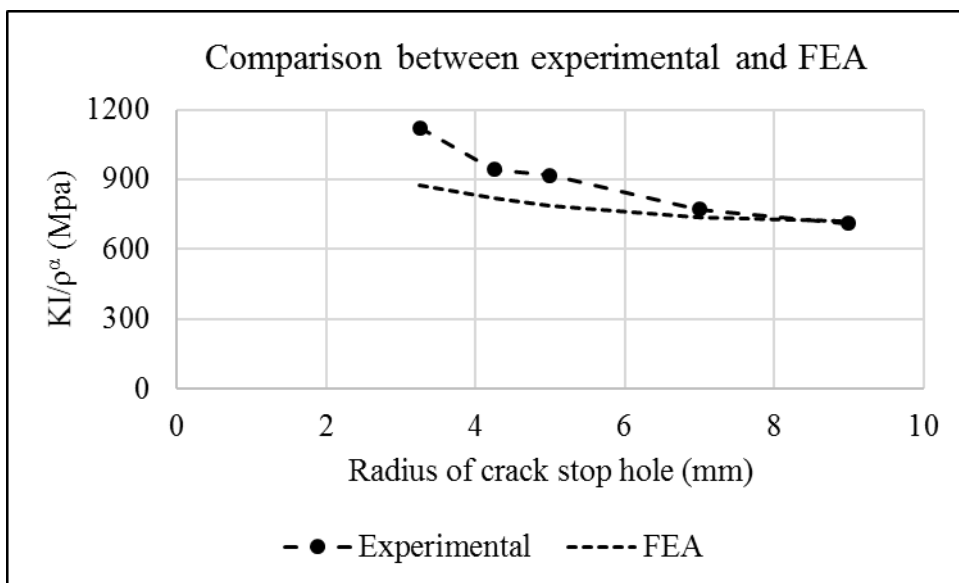


Figure 10 (b):  $KI/\rho^\alpha$  vs crack stop hole radii of single sided repair

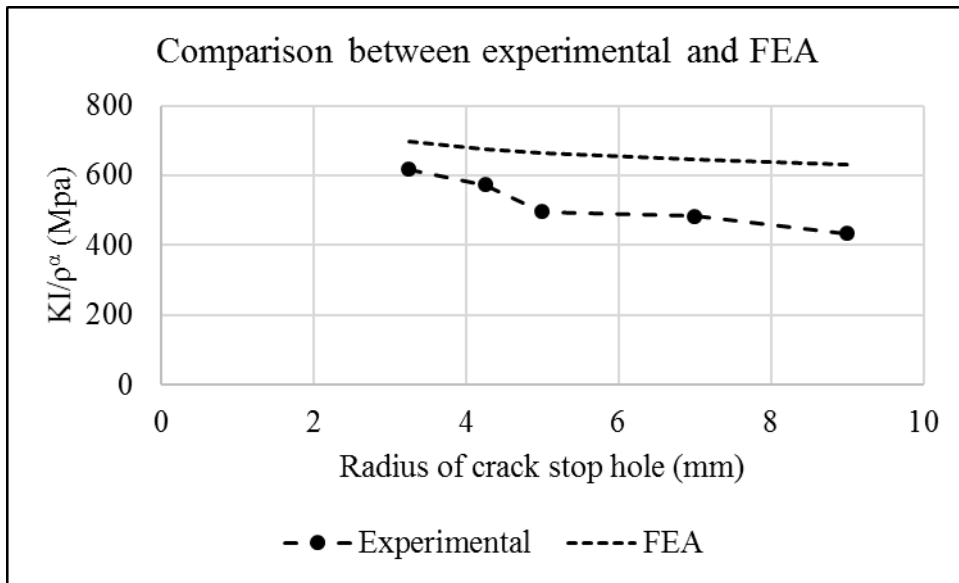


Figure 10 (c):  $KI/\rho^\alpha$  vs crack stop hole radii of double sided repair

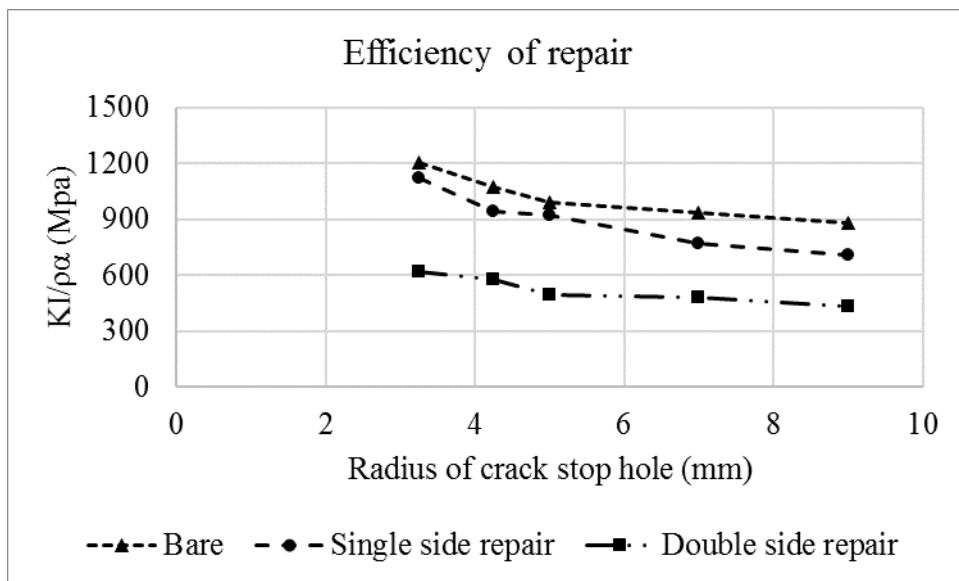


Figure 11:  $KI/\rho^\alpha$  vs crack stop hole radii of various repair techniques

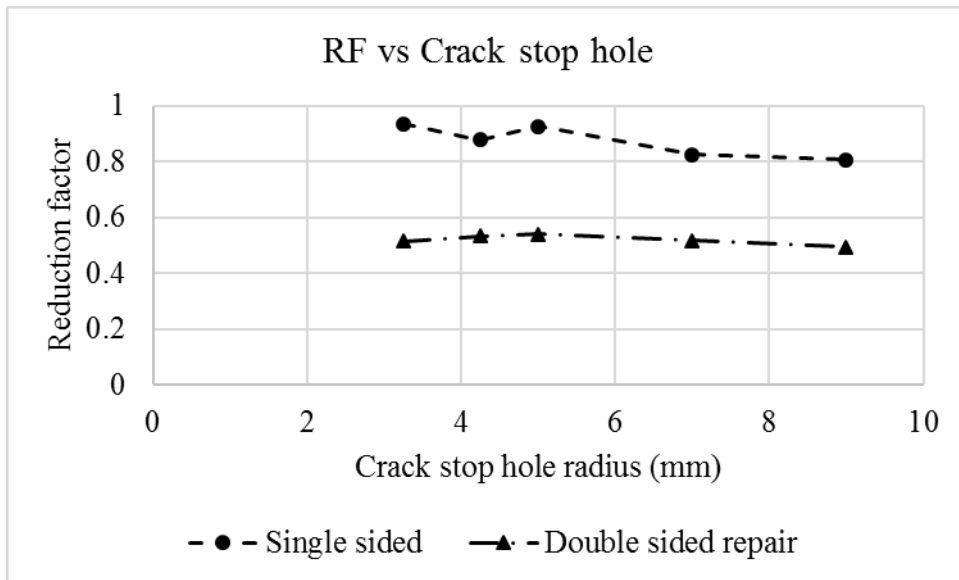


Figure 12: RF vs crack stop hole radii for one layer of CFRP

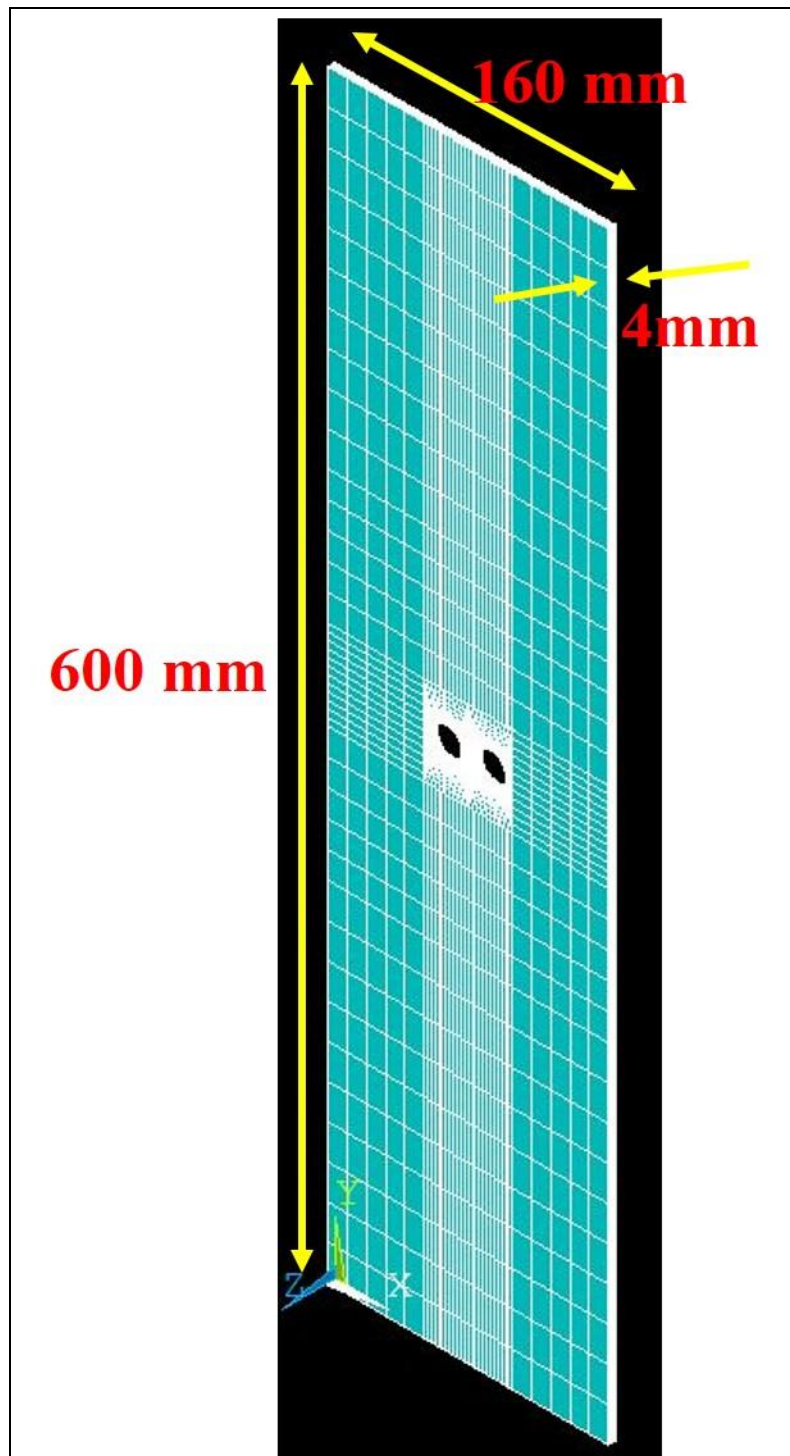


Figure 13: Geometry of the specimen in ANSYS

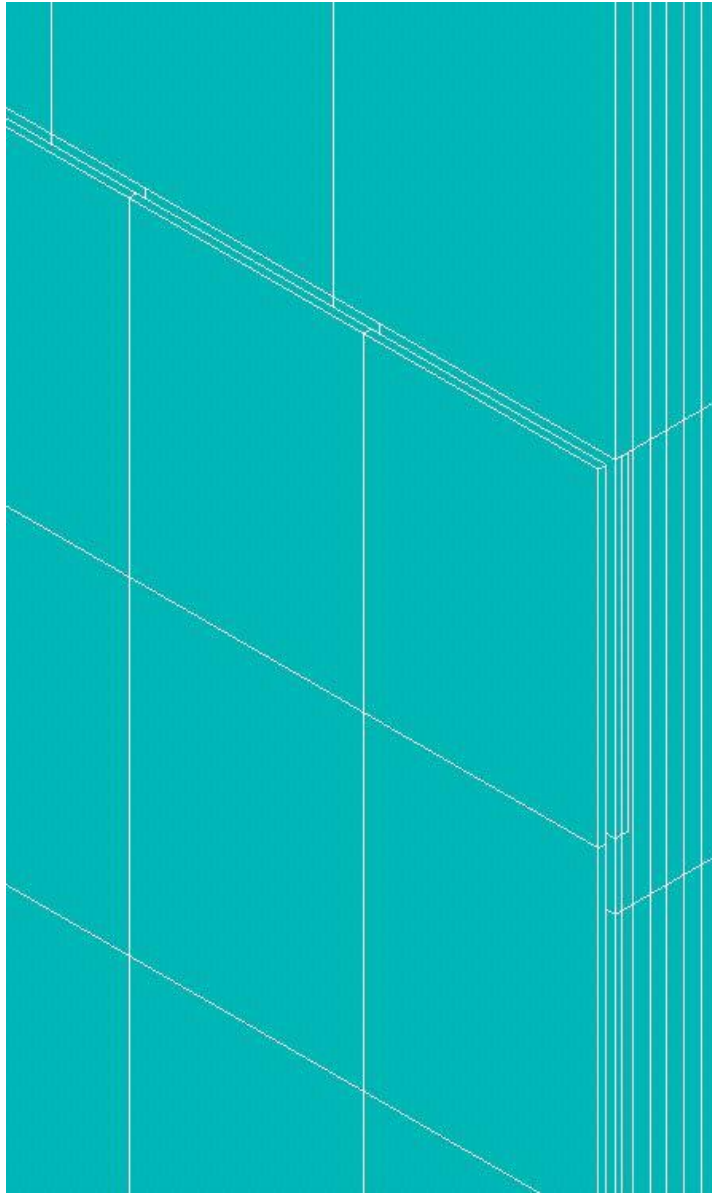


Figure 14 (a): Modelling of single sided specimen

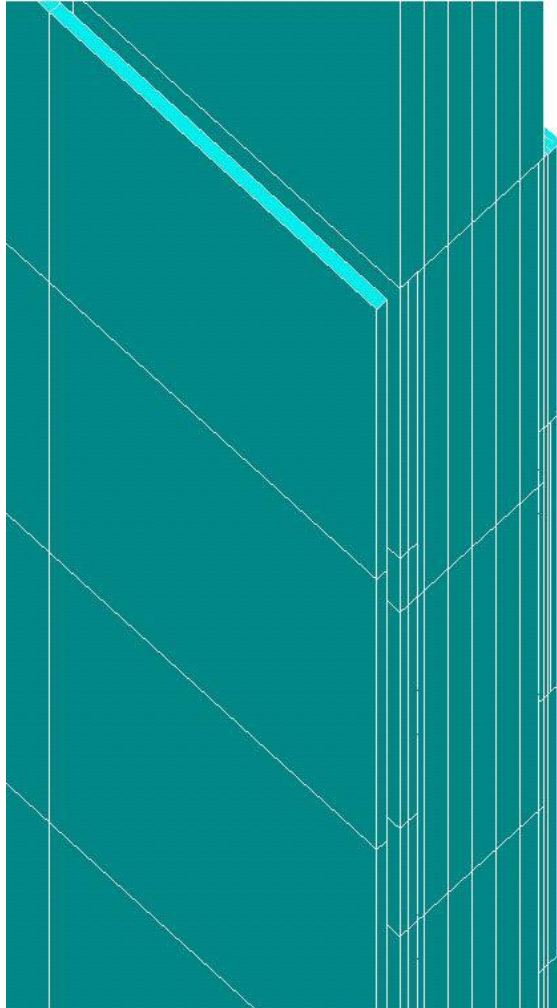


Figure 14 (b): FEA modelling of double sided specimen



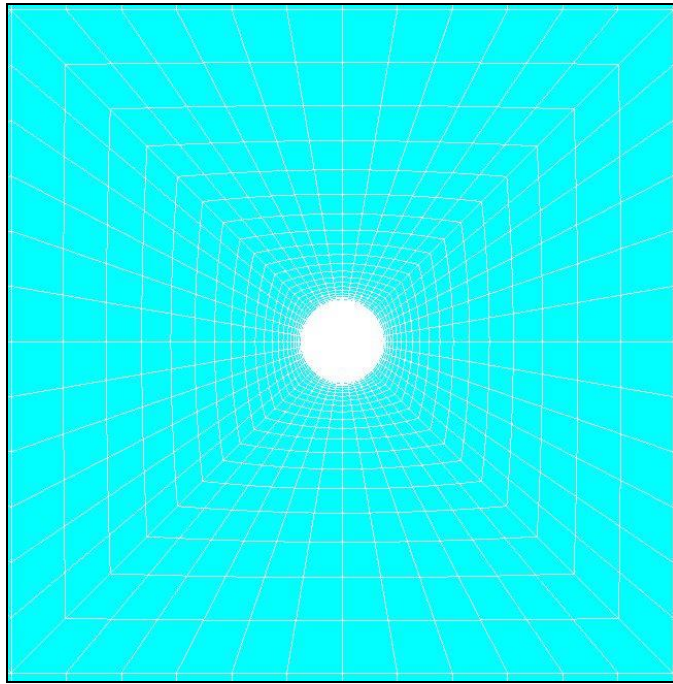


Figure 15(a): Meshing around the crack stop hole in radial and angular direction

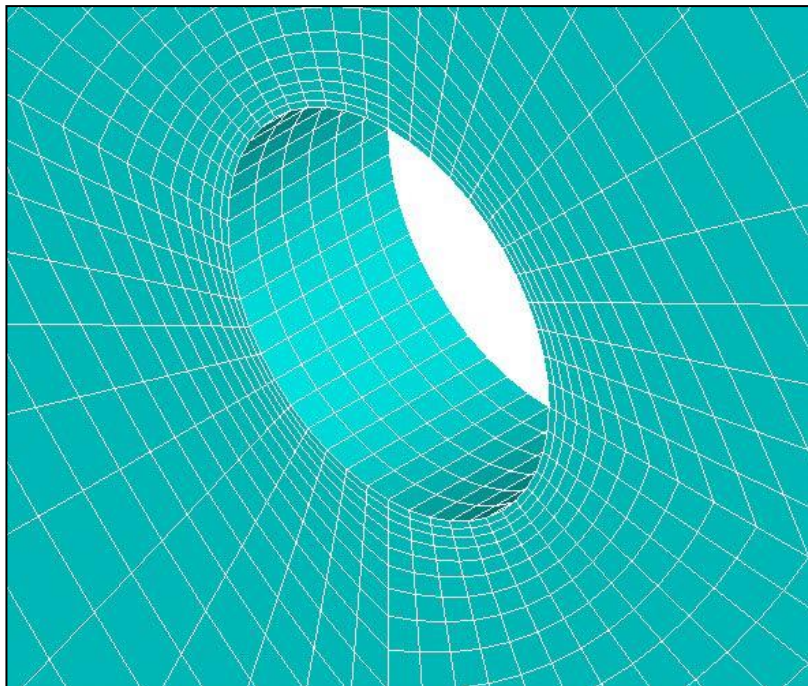


Figure 15(b): Meshing around the hole in thickness direction

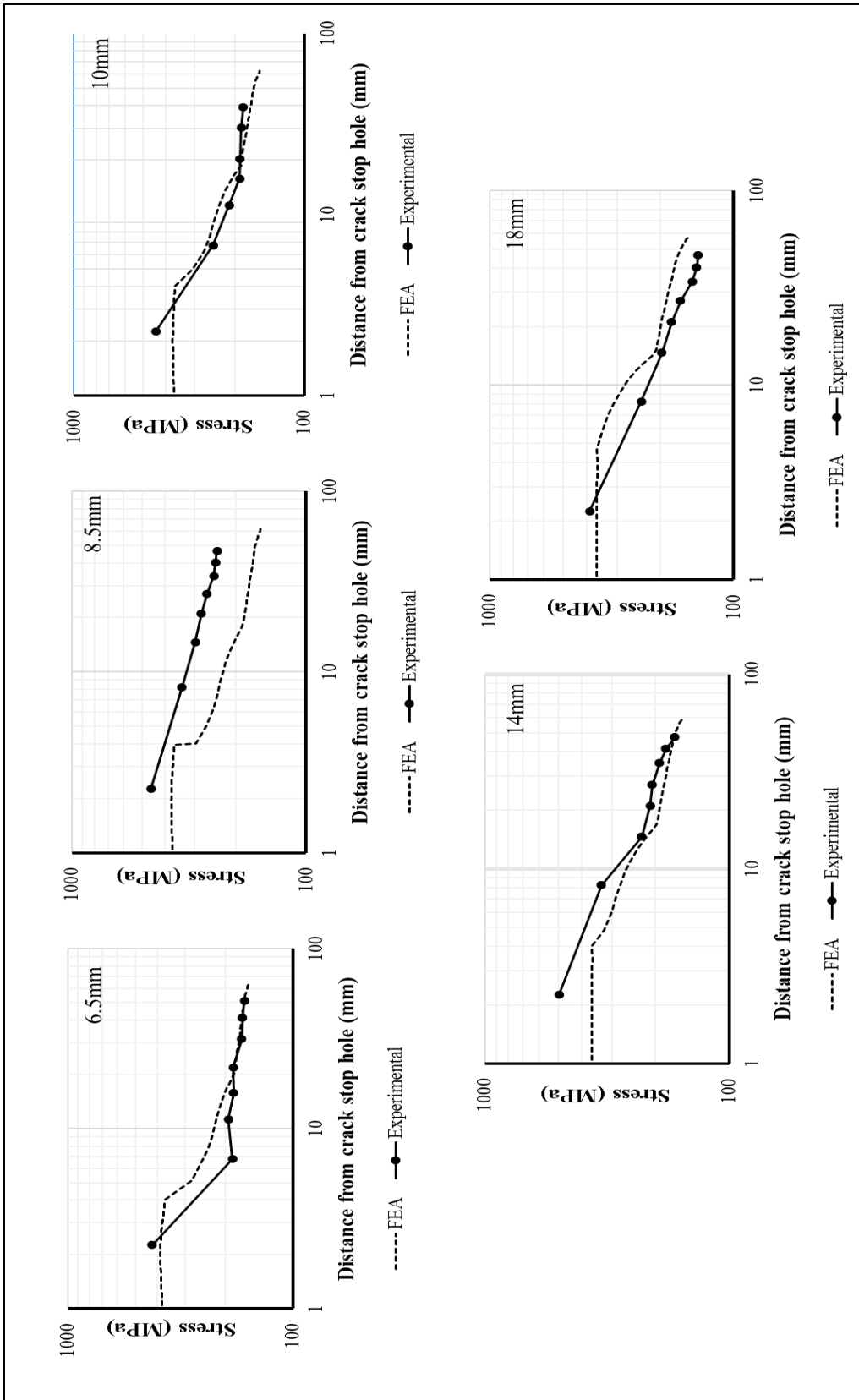


Figure 16: Alpha graphs for bare steel specimen

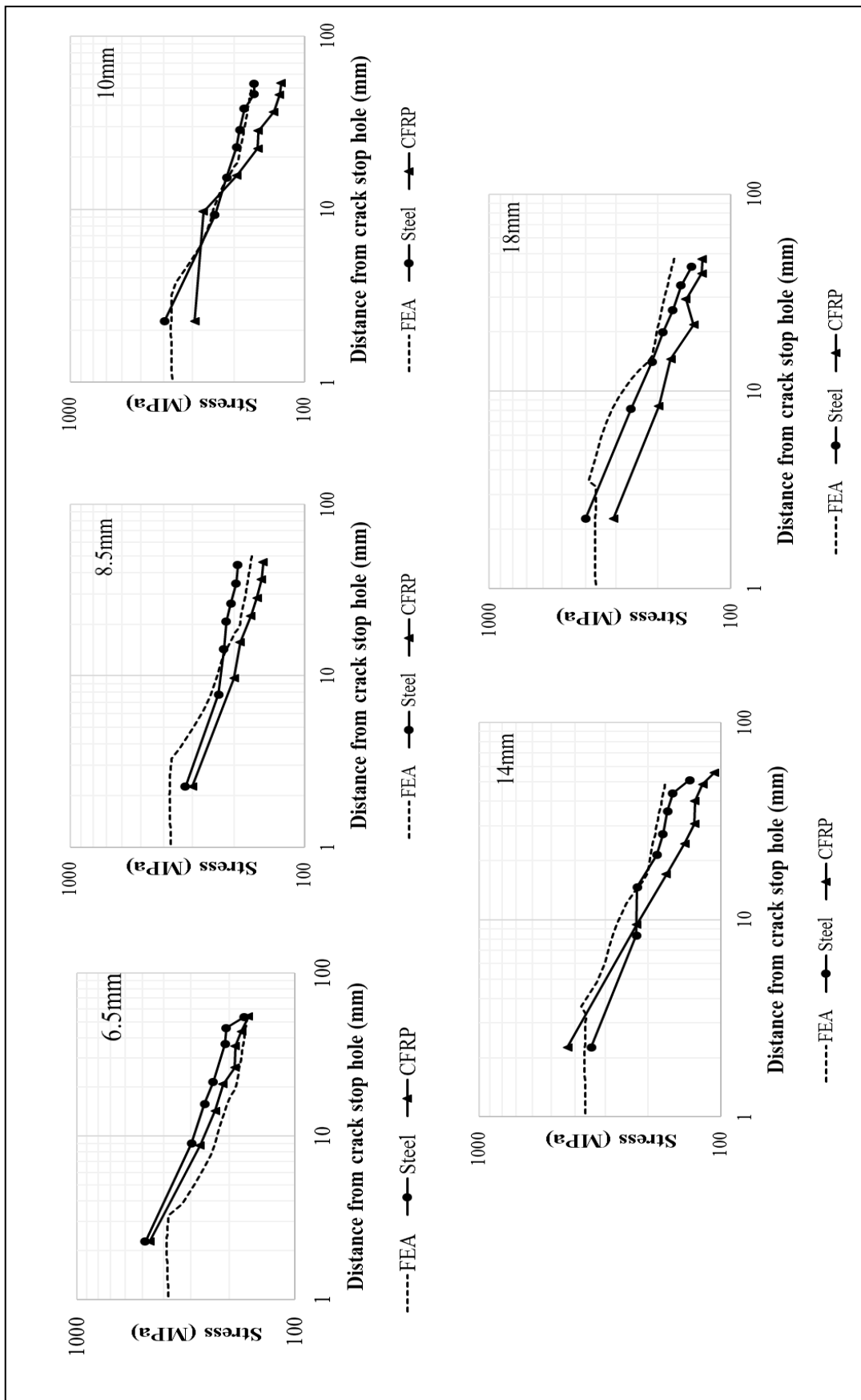


Figure 17: Alpha graphs for single side repaired specimen

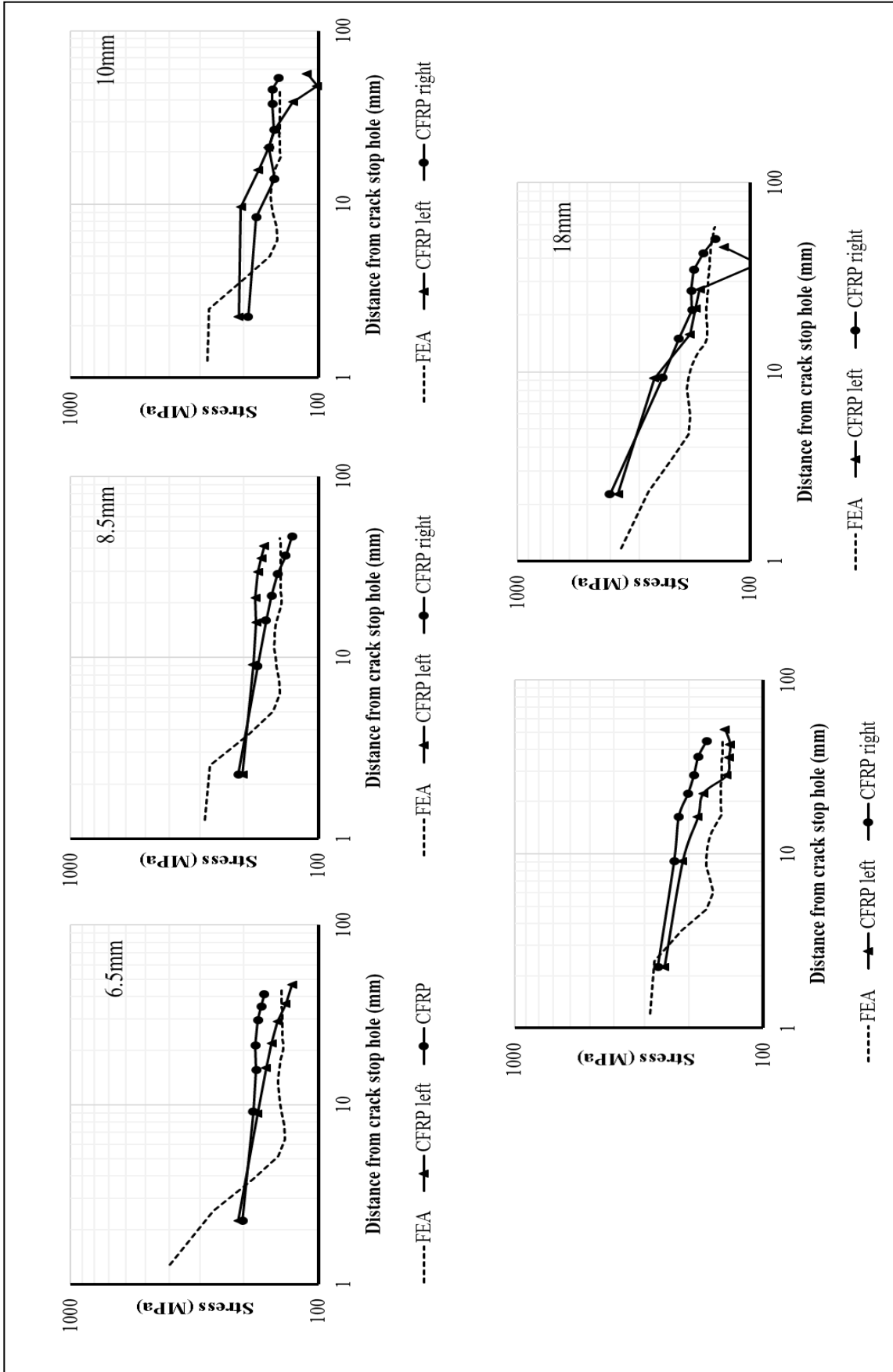


Figure 18: Alpha graphs for double side repaired specimen

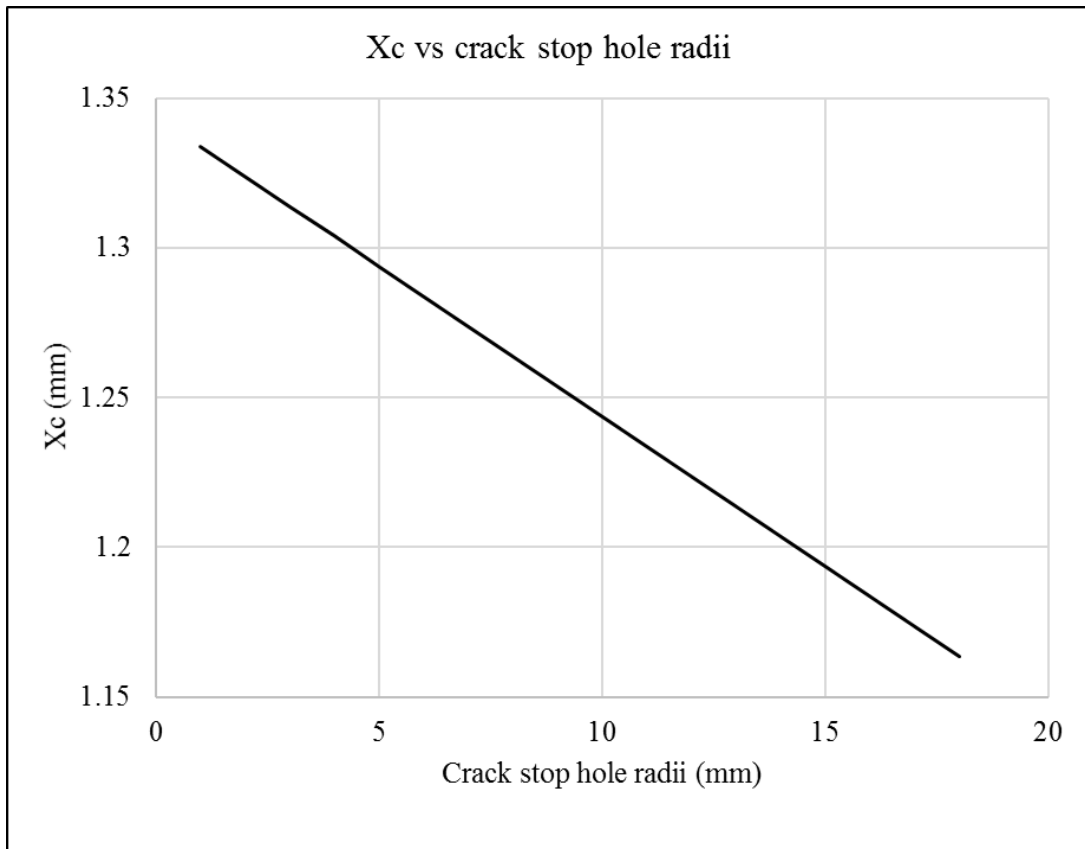


Figure 19: Calculation of  $X_c$  at desired crack stop hole radius